Control of a Group of Mobile Robots Based on Formation Abstraction and Decentralized Locational Optimization

Kazuya Yoshida, Hiroaki Fukushima, *Member, IEEE*, Kazuyuki Kon, *Member, IEEE*, and Fumitoshi Matsuno, *Member, IEEE*

***Abstract*—In this paper, we propose a new method of controlling a group of mobile robots based on formation abstraction. The shape of a formation is represented by a deformable polygon, which is constructed by bending a rectangle, to go through narrow spaces without colliding with obstacles. If the trajectory of the front end point, as well as the width and the length of the formation, are given, the formation automatically reshapes itself to fit the area through which the front part of the group has already safely passed. Furthermore, the robots continuously try to optimize their positions to decrease the risk of collisions by integrating a decentralized locational optimization algorithm into the formation control. We show that the objective function, taking into account the distance between robots, does not decrease for fixed and nonconvex polygonal formation shapes if the zero-order hold control is applied for a sufficiently short sampling period. We also analyze the influence of the decentralized locational optimization algorithm on the objective function in the case of variable formations. The effectiveness of the proposed method is demonstrated in both simulations and real robot experiments.**

***Index Terms*—Decentralized control, formation abstraction, formation control, locational optimization.**

I. Introduction

COORDINATION of multiple mobile robots has been a significant field of research for possible applications such as exploration, surveillance, mapping of unknown environments, and the transport of large objects (see, e.g., [1]–[3] for an overview). This paper focuses on the fundamental problem of moving a number of robots as a whole to a target area. The literature contains several types of approaches to deal with this problem.

The virtual structure approach considers a group of robots as a single virtual rigid structure so that the whole group can be controlled similarly to a single object [4]–[6]. A limitation of this approach is the difficulty of reshaping the formation to adapt to avoid obstacles. In the leader–follower approach, the robots each maintain a given position relative to the leader [7]–[11]. Although the formation shape can adapt to the environment by appropriately changing the target positions of the followers relative to the leader, it becomes increasingly difficult to do so, as the number of robots in a team grows. More recent methods aim to contain the followers in a convex hull of multiple leaders' positions so that it is not necessary to give a target position to each follower [12], [13]. However, it is not clear how to adapt the leaders' positions dynamically depending on the environments, which becomes difficult as the number of leaders increases to handle complex environments and large numbers of followers.

The behavior-based approach aims to derive the overall behavior of a robot group by weighing the relative importance of several desired behaviors (e.g., collision avoidance, formation keeping, target seeking) prescribed for each robot [14]–[16]. While the control algorithms are relatively simple and decentralized, it is generally difficult to mathematically analyze the behavior of the overall system. On the other hand, a more recent approach that is based on biologically-inspired artificial potential functions and velocity consensus allows the overall system analysis using Lyapunov functions in environments without obstacles [17], [18]. However, the group is easily separated when encountering obstacles, and there is no guarantee it will reform coherently after that. A certain level of centralization might be inevitable to control a number of robots as a whole, especially in complex environments that contain obstacles.

The approach most closely related to the one we use in this paper is based on formation abstraction, which was first introduced in [19]. The whole group of robots is represented by a simple geometric shape, such as a rectangle or an ellipsoid. The control method in [19] aims to keep a group of point robots inside a given geometric shape, which is dynamically changing. However, the control method does not take into account the relative distances between robots. Thus, some robots might become significantly closer to each other as the formation reshapes, even if the area of the shape is maintained.

More recent studies on formation abstraction introduce a velocity constraint [20] or an additional feedback law [21], [22] for

Manuscript received April 29, 2013; revised September 8, 2013; accepted December 1, 2013. Date of publication December 23, 2013; date of current version June 3, 2014. This paper was recommended for publication by Associate Editor C. C. Cheah and Editor G. Oriolo upon evaluation of the reviewers' comments. This paper was supported in part by the Ministry of Education, Culture, Sports, Science, and Technology Grant-in-Aid for Scientific Research (No. 24560546).

K. Yoshida is with the Caterpillar Japan ltd., Hyogo 674-8686, Japan (e-mail: kzy.yoshida@gmail.com).

H. Fukushima, K. Kon, and F. Matsuno are with the Department of Mechanical Engineering and Science, Graduate School of Engineering, Kyoto University, Kyoto daigaku-Katsura, Nishikyo-ku, Kyoto 615-8540, Japan (e-mail: fuku@me.kyoto-u.ac.jp; kon@me.kyoto-u.ac.jp; matsuno@me.kyoto-u.ac.jp).

This paper has supplementary downloadable material available at http://ieeexplore.ieee.org.

Color versions of one or more of the figures in this paper are available online at http://ieeexplore.ieee.org.

Digital Object Identifier 10.1109/TRO.2013.2293836

each robot to move away from other robots inside a prescribed safety region. For such decentralized feedback laws based on local information, it is inevitably difficult to guarantee that the requirements of both collision avoidance and formation shape control are satisfied, since these requirements often conflict with each other. Since it is difficult for any decentralized collision avoidance methods including the method in this paper to overcome this limitation, actions to decrease the risk of collisions should be started before other robots enter the safety region.

Another limitation of existing studies on formation abstraction is that they have not fully discussed how the formation should be deformed in certain situations. In [19] and [20], the situations where a robot group changes the width of a rectangular or ellipsoidal formation to go through narrow paths was discussed. However, more flexibility of the formation is required to move in complex environments. For example, in order for a large group to make a turn in narrow corners, the formation must be able to bend.

One way for a large group to go through a narrow space without colliding with obstacles is to form a long slender shape and bend the formation to fit the area through which the front part of the group has already safely passed. As a result, if the front part of the group does not collide with obstacles, the following parts can pass through the same area without collision. Similar strategies have been adopted in the operation of snakelike robots, which are typically composed of three or more segments connected serially, to search narrow spaces [23]–[25]. Human operators are required to command only one unit in the front part of the robot; then, commands for the joint angles are automatically calculated for the rest of the units to track the path of the preceding unit.

In this paper, we propose a new method of controlling a group of mobile robots based on formation abstraction. In rectangular formations, we use a polygonal formation that can bend to go through narrow spaces without colliding with obstacles. A polygonal formation is constructed based on a serial link in the middle of the formation. The polygon is bent by changing the joint angles of the serial link. The existing methods [23]–[25] for snakelike robots can be used to determine the joint angles, such that each link tracks the path of the preceding link. Therefore, if the trajectory of the front end point as well as the width and the length of the formation are given, the formation automatically reshapes to fit the area through which the front part of the formation has already safely passed.

Another feature of the proposed method compared with the existing methods in [19]–[22] is that actions to decrease the risk of collisions are started before other robots enter the safety region prescribed for collision avoidance. If the distances between robots are larger, the robots have a lower risk of collision in the future. Likewise, if the distances from robots to the boundary of the polygonal region of formation are larger, the robots have a lower risk of going out of the region in the future. Thus, we consider the objective function which is defined as the minimum of the distances between robots and the distances from robots to the boundary of the polygonal region, in order to quantify the risk of violation of the requirements of collision avoidance and formation shape control. In the proposed method, all the robots continuously try to achieve the optimal disposition in which the objective function is maximized. To this end, we integrate a decentralized locational optimization algorithm [26] into formation control. More precisely, a decentralized locational optimization algorithm [26] developed for static convex environments is extended to apply to dynamically changing nonconvex environments. Due to the nonsmooth and decentralized properties of the control law, it is not straightforward to guarantee the optimality of the robot positions even in cases where the formation shape is fixed and convex. Thus, we show that the objective function does not decrease for fixed and nonconvex polygonal formation shapes if the zero-order hold control is applied for a sufficiently short sampling period. In the variable formation case, the cost function is not necessarily nondecreasing. Thus, we aim to show that the additional input for the locational optimization makes the value of the cost function greater than its value without this input. The effectiveness of the proposed method is demonstrated in both simulations and real robot experiments.

II. Control Objective

Consider n robots with the following kinematic model:

$$\dot{q}_i = u_i, \quad i = 1, \ldots, n \tag{1}$$

where $q_i \in \mathbb{R}^2$ and u_i are the absolute position and the control input of the robot i, respectively. The set of robots closest to robot $i \in \{1, \ldots, n\}$ is defined as

$$\mathcal{N}_i := \left\{ j_i \;\middle|\; \|q_i - q_{j_i}\| = \min_{j \neq i} \|q_i - q_j\| \right\}. \tag{2}$$

It is assumed that the robot $i \in \{1, \ldots, n\}$ knows its own position q_i and the relative position $q_{j_i} - q_i$ of each nearest robot $j_i \in \mathcal{N}_i$. This implies that there is always at least one robot in the sensing region of every robot. This assumption should be valid, since robots do not go far away from the nearest robots, as long as all robots are inside the abstracted formation shape, as described in Section II-A.

A. Formation Abstraction

By formation abstraction, we mean that the gross position and orientation as well as the shape of a group of robots are described by a smaller number of states, which are called abstract states, than the dimension $2n$ of $Q := [q_1^T, \ldots, q_n^T]^T$. More precisely, the group is represented by a simple geometric shape, inside of which each robot is controlled to maintain. Although the number of abstract states should not depend on n in the original definition of formation abstraction [19], it might be inevitable that the number of abstract states depends on n in cases where the formation shape deforms to adapt to complex environments. Thus, we aim to achieve formation abstraction exhibiting two properties: 1) Only a few abstract states independent of n need to be chosen according to the information on the environments, and 2) the rest of the abstract states are automatically determined by a prescribed algorithm according to the few abstract states given as 1).

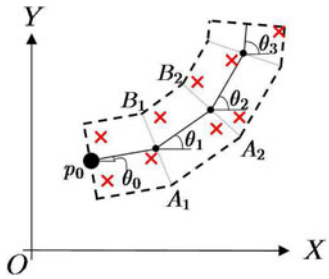

Fig. 1. Polygonal region $\mathcal{P}$.

We consider a formation shape described by the polygon $\mathcal{P}$ as shown by the dashed line in Fig. 1. To construct the polygon $\mathcal{P}$, we first consider a serial-link structure as shown in the middle of the polygon in Fig. 1. Let σ_1 be the sum of the lengths of all the links, and the length of each link except for the last link is assumed to be given as a constant L. Then, the number of links is defined as $m := \lceil \sigma_1/L \rceil$, and the length of the last link is $\sigma_1 - (m-1)L$. The front end of the serial-link structure is located at p_0, and the orientation of each link is defined as θ_k $(k = 0, 1, \ldots, m-1)$.

Two of the edges of the polygon in Fig. 1 are orthogonal to the first and the last links, respectively. The rest of the edges are parallel to one of the links and have a distance $\sigma_2/2$ from the link. Such relationships between the polygon and the serial link are always maintained, when the formation reshapes. One way to change the shape of the formation is to change the relative angles between adjacent links, i.e., $\theta_k - \theta_{k-1}$ $(k = 1, \ldots, m)$. This is called a bending operation. In special cases, where $\theta_0 = \theta_1 = \cdots = \theta_{m-1}$, the formation shape is a rectangle, which has length σ_1 and width σ_2. Another way to change the shape of the formation is to change σ_1 and σ_2. When the group goes into a narrow space, the width σ_2 should be decreased, while the length σ_1 is accordingly increased to maintain the area of the polygon so that it can accommodate all the robots. The target value of $\sigma := [\sigma_1, \sigma_2]^T$ is defined as $\sigma_d = [\sigma_{d1}, \sigma_{d2}]^T$. If σ_d is given, then σ can be easily determined such that σ converges to σ_d, for example, by $\dot{\sigma}_1 = K_1(\sigma_{d1} - \sigma_1)$ and $\dot{\sigma}_2 = K_2(\sigma_{d2} - \sigma_2)$, where K_1 and K_2 are given positive constants.

In this paper, we assume that p_0, θ_0, and σ_d are given by for example a human operator who has information on the environments. One way for the formation to go through a narrow space without colliding with obstacles is to control θ_k $(k = 1, \ldots, m-1)$ such that each link in the middle of the formation tracks the path of the preceding link. In such cases, it is expected that the whole group can avoid collisions with obstacles, if p_0, θ_0, and σ_d are appropriately chosen such that the serial-link structure avoids obstacles with a margin of at least σ_{d2}. Some algorithms are proposed in the literature [23]–[25] in order to determine joint angles θ_k $(k = 1, \ldots, m-1)$, for the front-link tracking. Thus, we do not focus on how to determine θ_k $(k = 1, \ldots, m-1)$. The method in [24], which is summarized in Appendix A, is used without any modifications in simulations and experiments. In order to have the method in [24] work as intended, the first link is not allowed to move backwards or sideways. More precisely, the trajectories of p_0 and θ_0 are determined such that

$$\dot{p}_0 = -\begin{bmatrix} v_0 \cos\theta_0 \\ v_0 \sin\theta_0 \end{bmatrix}, \quad \dot{\theta}_0 = \omega_0 \tag{3}$$

where p_0 is allowed to move forward only, i.e., $v_0 > 0$. This implies that we consider situations where the command of (v_0, ω_0) is given by the operator. Using (v_0, ω_0), the trajectory of $(p_0(t), \theta_0(t))$ is generated from (3) and the given initial value $(p_0(0), \theta_0(0))$. In addition, the joint angles are limited as follows, similar to [24]:

$$|\theta_k - \theta_{k-1}| \le \pi/2, \quad k = 1, \ldots, m-1. \tag{4}$$

As shown in Fig. 3, we assume that $\theta := [\theta_0, \ldots, \theta_{m-1}]^T$ and σ are determined from p_0, θ_0, and σ_d by the abstract motion planner on a central computer and that p_0, θ and σ are broadcast to each robot. The main focus in this paper is the control of Q using (p_0, θ, σ).

To derive a control law that maintains all the robots in $\mathcal{P}$, we introduce the coordinate transformation $T_{(p_0,\theta)}$ from q to $z = [r, l]^T$ in the r–l frame as shown in Fig. 2. The subscript "(p_0, θ)" indicates that $z = T_{(p_0,\theta)}(q)$ depends on p_0 and θ, as well as on q. Roughly speaking, l in Fig. 2 represents the deviation from the closest link, while r represents the deviation from p_0 measured along the links. The points (A_1, A_2, B_2, B_1) in Fig. 1 are mapped to (A_1', A_2', B_2', B_1') in Fig. 2. In order to simplify the transformation, we assume that the joint angle and σ_2 satisfy the following assumption:

$$|\theta_k - \theta_{k-1}| \le 2\tan^{-1}\frac{L}{\sigma_2}, \quad k = 1, \ldots, m-1. \tag{5}$$

Under this assumption, the polygon $\mathcal{P}$ is always divided into m trapezoids. The details on the transformation $T_{(p_0,\theta)}$ are described in Appendix B. We define the rectangular region in Fig. 2 as

$$\mathcal{R} := \{[r, l]^T \in \mathbb{R}^2 \mid 0 < r \le \sigma_1, |\, l \,| < \sigma_2/2\}. \tag{6}$$

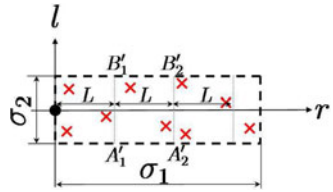

Fig. 2. Rectangular region $\mathcal{R}$.

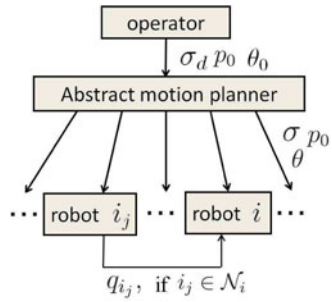

Fig. 3. Information flow.

Then, $q \in \mathcal{P}$ if and only if $z \in \mathcal{R}$.

One of our control objectives, which we refer to as the main task, is to keep all the robots in the polygon $\mathcal{P}$, while σ, p_0, and θ are changed. It is assumed that σ_1 and σ_2 are chosen such that $q_i \in \mathcal{P}$ for any robot $i \in \{1, \ldots, n\}$ at the initial time. We also assume that $q_i(0) \neq q_j(0)$ for any $j \in \{1, \ldots, n\} \setminus \{i\}$.

B. Locational Optimization

Another control objective, which we call the subtask, is to decrease the risk of collisions by keeping as long distance as possible between robots as well as between a robot and the boundary of $\mathcal{P}$. In other words, the subtask aims to keep the density of robots as uniform as possible over $\mathcal{P}$.

In order to represent the minimum distance from the robot $i \in \{1, \ldots, n\}$ to other robots or the boundary of $\mathcal{P}$, we define

$$H_i(V) := \min_{q \in \mathcal{M}_i} \|q_i - q\|, \quad i = 1, \ldots, n \tag{7}$$

where

$$\begin{aligned} V &:= [Q^T, \sigma^T, \theta^T, p_0^T]^T \\ \mathcal{M}_i &:= \partial\mathcal{P} \cup \bigcup_{j_i \in \mathcal{N}_i} \left\{ \frac{1}{2}(q_i + q_{j_i}) \right\} \end{aligned} \tag{8}$$

and $\partial\mathcal{P}$ is the boundary of $\mathcal{P}$. Note that $\partial\mathcal{P}$ generally depends on (σ, θ, p_0) so that $H_i(V)$ is a function of these variables as well as of Q. It is also important to note that half of the distance between two robots is considered in (7), since twice the distance is needed to prevent the collision with other robots compared with the collision with the boundary of $\mathcal{P}$. This is because a robot needs to take into account the size of another robot as well as its own size in order to avoid colliding with other robots. By using (7), we define the following objective function for the whole group:

$$\mathcal{H}(V) := \min_{i \in \{1, \ldots, n\}} H_i(V). \tag{9}$$

We introduce a control law which aims to increase the value of $\mathcal{H}(V)$ as much as possible for a given (σ, θ, p_0) by controlling Q. In the case of point robots, each robot does not collide with other robots and the boundary of $\mathcal{P}$, if $\mathcal{H}(V)$ is not decreasing, because of the assumption that $q_i(0) \in \mathcal{P}$ and $q_i(0) \neq q_j(0)$ $(i \in \{1, \ldots, n\}, j \in \{1, \ldots, n\} \setminus \{i\})$. For real robots, the relationship between $\mathcal{H}(V)$ and collision avoidance is described in the following remark.

Remark 1 In the case of real robots, q_i is the position of a fixed representative point on the robot i $(i = 1, \ldots, n)$. Once a representative point is fixed for each robot, we can determine a positive constant γ from the shapes of the robots, such that the circle of radius γ centered at q_i includes the whole body of the robot i for each $i = 1, \ldots, n$. Suppose $\mathcal{H}(V) > 2\gamma$ is initially satisfied. Then, if $\mathcal{H}(V)$ is not decreasing, it is guaranteed that no collision occurs between robots and that the whole body of each robot is inside $\mathcal{P}$.

III. Control Method

The control input for each robot can be divided into two components, as follows:

$$u_i = u_{mi} + u_{si}, \quad i = 1, \ldots, n \tag{10}$$

where u_{mi} and u_{si} are the control inputs for the main task and the subtask, respectively.

A. Control Law for the Main Task

The control input u_{mi} for the main task is given such that $z_i = T_{(p_0, \theta)}(q_i)$ satisfies

$$\dot{r}_i = \frac{r_i}{\sigma_1}\dot{\sigma}_1, \quad \dot{l}_i = \frac{l_i}{\sigma_2}\dot{\sigma}_2, \quad i = 1, \ldots, n \tag{11}$$

when $u_i = u_{mi}$. See Appendix C for the explicit form of u_{mi}. As shown in the following proposition, the input $u_i = u_{mi}$ keeps z_i in $\mathcal{R}$, which implies $q_i \in \mathcal{P}$.

Proposition 1: For the system in (11), we have $0 < r_i(t) < \sigma_1(t), |\, l_i(t) \,| < \sigma_2(t)/2, \forall t > 0$, if it is satisfied at $t = 0$.

Proof: From (11), we have $\frac{d}{dt}(\frac{r_i}{\sigma_1}) = 0$. Thus, it holds that $r_i(t) = c\sigma_1(t)$ for some constant c. Since $0 < r_i(0) < \sigma_1(0)$, we have $0 < c < 1$. Therefore, since $\sigma_1(t) > 0$ for any $t > 0$, we obtain $0 < r_i(t) < \sigma_1(t)$ for any $t > 0$. Similarly, $\frac{d}{dt}(\frac{l_i}{\sigma_2}) = 0$ is obtained from (11), which implies $l_i(t) = c\sigma_2(t)$ for some constant c. Since $|l_i(0)| < \sigma_2(0)/2$, we have $|c| < 1/2$, which implies $|l_i(t)| < \sigma_2(t)/2$ for any $t > 0$. ■

In the same way, if $z_i(0) \neq z_j(0)$ for another robot $j \in \{1, \ldots, n\} \setminus \{i\}$, it can be proved that $z_i(t) \neq z_j(t)$ for any $t > 0$. This implies that $q_i(t) \neq q_j(t)$ for any $t > 0$ if $q_i(0) \neq q_j(0)$, since $T_{(p_0, \theta)}$ is a one-to-one transformation from q to z. From this fact and Proposition 1, we can see that $\mathcal{H}(V(t)) > 0$ at any $t > 0$ if $\mathcal{H}(V(0)) > 0$. Thus, in the case of point robots, no collision occurs even if $u_{si} = 0$. However, unlike point robots, real robots collide when their positions are too close, even if $z_i(t) \neq z_j(t)$. The following example shows a situation where the positions of two robots easily become close.

Example 1: Consider a rectangular formation changing the width and length as $\dot{\sigma}_1 > 0$ and $\dot{\sigma}_2 < 0$, respectively. Without a loss of generality, we assume that $p_0 = 0_2$ and $\theta_0 = 0$, where 0_ℓ denotes the ℓ dimensional zero vector for a natural number ℓ, throughout the paper. In this case, the closed-loop system for the robot i without u_{si} is described as

$$\dot{X}_i = \frac{X_i}{\sigma_1}\dot{\sigma}_1, \;\; \dot{Y}_i = \frac{Y_i}{\sigma_2}\dot{\sigma}_2, \;\; i = 1, \ldots, n \tag{12}$$

where (X_i, Y_i) is the XY coordinate of q_i. Thus, the relative position of the robot i with another robot $j \in \{1, \ldots, n\} \setminus \{i\}$ is changed as follows:

$$\dot{X}_i - \dot{X}_j = \frac{X_i - X_j}{\sigma_1}\dot{\sigma}_1, \quad \dot{Y}_i - \dot{Y}_j = \frac{Y_i - Y_j}{\sigma_2}\dot{\sigma}_2. \tag{13}$$

The distance between two robots i and j in the Y-direction, $|Y_j - Y_i|$, is obviously decreased due to $\dot{\sigma}_2 < 0$. This implies that the two robots, whose X-coordinates are close, i.e., $X_i \simeq X_j$, could collide, even if the Y-coordinates of the robots i and j are initially large enough to avoid collision. In order to avoid both collisions and achieve the target formation shape

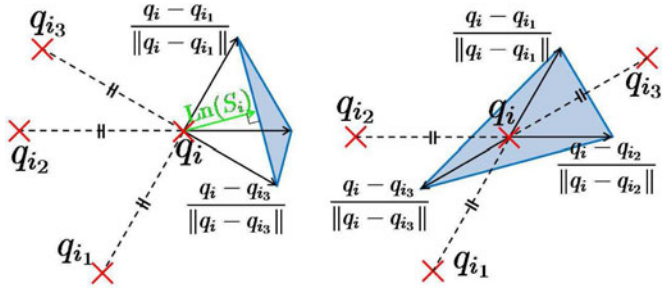

Fig. 4. Schematic of $\mathrm{Ln}(S_i)$ (left: $0_2 \notin S_i$, right: $0_2 \in S_i$), where S_i is the set of vectors from q_i to all points on the colored triangle region.

in this case, the distance in the X-direction $|X_i - X_j|$ has to be increased. However, since $X_i \simeq X_j$, almost no change is made to $|X_i - X_j|$, as seen in (13). In other words, although an additional space is generated in the X-direction due to $\dot{\sigma}_1 > 0$, the two robots, which are close to each other in the X-direction, do not use the additional space and remain close to each other.

The limitation of the control input $u_i = u_{mi}$, as described in Example 1, is also shown in the simulation of Section V-B. To overcome the limitation of $u_i = u_{mi}$, we next introduce an additional control law that always tries to optimize the positions of the robots in formation.

B. Control Law for the Subtask

For the locational optimization in the nonconvex region as described in Section II-B, we generalize the control method in [26] for convex regions as follows:

$$u_{si} = \hat{K} \cdot \mathrm{Ln}\left(S_i\right), \quad i = 1, \ldots, n \tag{14}$$

$$S_i := \mathrm{co}\left\{ \frac{q_i - q^*}{\|q_i - q^*\|} \middle| q^* \in \underset{q \in \mathcal{M}_i}{\arg\min} \|q_i - q\| \right\} \tag{15}$$

where $\hat{K}$ is a positive constant, $\mathrm{co}(S)$ denotes the convex hull of a set $S \subset \mathbb{R}^2$, and $\mathrm{Ln}(S)$ is the least-norm element of the closure $\bar{S}$ of S, i.e., $\mathrm{Ln}(S) := \mathrm{argmin}_{v \in \bar{S}} \|v\|$.

Roughly speaking, the control law in (14) aims to move the robot i away from the convex hull of the closest points in $\mathcal{M}_i$. If the convex hull of the closest points includes q_i, the input u_{si} becomes 0_2. Fig. 4 illustrates $\mathrm{Ln}(S_i)$ in the case where three points $\{q_{i_1}, q_{i_2}, q_{i_3}\}$ in $\mathcal{M}_i$ are closest to q_i. Fig. 4 (left) illustrates a case where S_i does not contain 0_2, while Fig. 4 (right) illustrates a case where S_i contains 0_2. We next rewrite (15) using the information on the edges of $\mathcal{P}$.

Let $\mathrm{Ed}(\mathcal{P}) := \{e_1, \ldots, e_M\}$ denote the set of edges of $\mathcal{P}$ when the number of edges is M. We denote by $\mathrm{Cp}_e(q_i)$ the closest point from q_i to the edge $e \in \mathrm{Ed}(\mathcal{P})$. Note that if three regions $D_L := \{q \in \mathbb{R}^2 \mid (q - v_L) \cdot (v_R - v_L) \leq 0, (q - v_R) \cdot (v_L - v_R) \geq 0\}$, $D_M := \{q \in \mathbb{R}^2 \mid (q - v_L) \cdot (v_R - v_L) \geq 0, (q - v_R) \cdot (v_L - v_R) \geq 0\}$, and $D_R := \{q \in \mathbb{R}^2 \mid (q - v_L) \cdot (v_R - v_L) \geq 0, (q - v_R) \cdot (v_L - v_R) \leq 0\}$ are defined using the coordinates of the vertices v_L and v_R of e, $\mathrm{Cp}_e(q_i)$ can be written as

$$\mathrm{Cp}_e(q_i) = \begin{cases} v_L, & \text{if } q_i \in D_L \\ v_L + \dfrac{(q_i - v_L) \cdot (v_R - v_L)}{\|v_R - v_L\|^2}(v_R - v_L), & \text{if } q_i \in D_M \\ v_R, & \text{if } q_i \in D_R. \end{cases} \tag{16}$$

By using $\mathrm{Cp}_e(q_i)$ above, H_i in (7) is rewritten as

$$H_i(V) = \min\left\{ \min_{j_i \in \mathcal{N}_i} F_{(i,j_i)}(V), \min_{e \in \mathrm{Ed}(\mathcal{P})} G_{(i,e)}(V) \right\} \tag{17}$$

where

$$F_{(i,j)}(V) := \frac{1}{2}\|q_i - q_j\|, G_{(i,e)}(V) := \|q_i - \mathrm{Cp}_e(q_i)\|.$$

Then, $\mathrm{argmin}_{q \in \mathcal{M}_i} \|q_i - q\|$ in (15) can be rewritten as

$$\underset{q \in \mathcal{M}_i}{\mathrm{argmin}} \|q_i - q\| = \left\{ \frac{q_i + q_{j_i}}{2} \middle| F_{(i,j_i)} = H_i, j_i \in \mathcal{N}_i \right\} \cup \left\{ \mathrm{Cp}_e(q_i) \middle| G_{(i,e)} = H_i, e \in \mathrm{Ed}(\mathcal{P}) \right\}.$$

Thus, S_i in (15) can be rewritten as

$$S_i = \mathrm{co}\left(\left\{ \frac{q_i - q_{j_i}}{\|q_i - q_{j_i}\|} \middle| F_{(i,j_i)} = H_i, j_i \in \mathcal{N}_i \right\} \cup \left\{ \frac{q_i - \mathrm{Cp}_e(q_i)}{\|q_i - \mathrm{Cp}_e(q_i)\|} \middle| G_{(i,e)} = H_i, e \in \mathrm{Ed}(\mathcal{P}) \right\} \right).$$

Therefore, u_{si} in (14) can be computed using the information on the nearest robots of the robot i and on a finite number of the edges of $\mathcal{P}$.

C. Relationship With Other Methods Using Abstraction

The existing method in [19] has a similar limitation to the control input $u_i = u_{mi}$ in Section III-A, which does not take into account the subtask. To illustrate this, we consider a simple case where the shape of the formation is changed without changing the gross position and orientation of the formation, in the same way as in Section III-A. Without a loss of generality, we assume that the gross position of the formation is located at the origin and that the orientation of the group is 0.

In [19], the variance $s = [s_1, s_2]^T$ of the robot positions is changed in order to control the formation shape, where

$$s_1 = \frac{1}{n-1}\sum_{i=1}^{n} X_i^2, \quad s_2 = \frac{1}{n-1}\sum_{i=1}^{n} Y_i^2. \tag{18}$$

To change s at the velocity $\dot{s}$, the control input vector $U := [u_1^T, \ldots, u_n^T]^T$ is given as

$$U = d\phi_s^T \left(d\phi_s d\phi_s^T\right)^{-1} \dot{s} \tag{19}$$

where

$$d\phi_s = \frac{1}{N-1}\begin{bmatrix} X_1 & 0 & \cdots & X_n & 0 \\ 0 & Y_1 & \cdots & 0 & Y_n \end{bmatrix}. \tag{20}$$

As a result, the closed-loop system for the robot i is

$$\dot{X}_i = \frac{X_i}{s_1}\dot{s}_1, \quad \dot{Y}_i = \frac{Y_i}{s}\dot{s}_2 \tag{21}$$

which has the same form as (12). Thus, the method in [19] suffers from the same problem as the one described in Example 1 when $\dot{s}_1 > 0$ and $\dot{s}_2 < 0$.

The method in [20] searches for the control input u_i ($i = 1, \ldots, n$) in (1), which satisfies two conditions, as follows. One of the condition is that

$$(q_i - q_j) \cdot (\dot{q}_i - \dot{q}_j) \geq 0 \tag{22}$$

is satisfied for each robot $j \in \{1, \ldots, n\} \setminus \{i\}$ in a given safety region. The robots in a given safety region are those at a distance shorter than a given value. The other condition is that the abstraction states, such as s, monotonically converge to the target values. However, it is difficult for the robot i to know $\dot{q}_j$ in (22), since $\dot{q}_j$ is determined by u_j, which the robot j searches for independently from u_i. Another limitation of this method is that the search for the control input satisfying both of the conditions is not always feasible, even if an estimate of $\dot{q}_j$ in (22) is available.

In [21] and [22], a repulsive force is applied to move away from the robots in a given safety region. If a robot is out of the target formation region, an attractive force to the region is applied. However, it is difficult to satisfy both the requirements of collision avoidance and formation shape control when these requirements conflict with each other. For example, if the width of the target region is decreased in the Y-direction similarly to the case in Example 1, the Y-coordinates of the robots tend to become close. In such cases, if the robot i has another robot j in the safety region and if $X_i \simeq X_j$, then the distance between the robots in the X-direction has to be increased rapidly to satisfy both requirements. However, it could take a long time for the distance in the X-direction to increase enough to avoid collisions, since the repulsive force in the X direction is small when $X_i \simeq X_j$.

In all the methods in [20]–[22], each robot tries to avoid colliding with other robots in a prescribed safety region. This type of collision avoidance methods might be unsuccessful for real robots, in cases where the requirements of collision avoidance and formation shape control conflict with each other. To address this problem, our method tries, as much as possible, to increase the minimum distance from other robots before those other robots enter the safety region. In the next section, we analyze the influence of the control law for the subtask in Section III-B on the value of $\mathcal{H}(V)$.

IV. Analysis of the Objective Function

A. Generalized Gradient of the Objective Function

The objective function $\mathcal{H}(V)$ in (9) is not differentiable in general, since the robot having the minimum value of $H_i(V)$ in (7) could be switched. Further, $H_i(V)$ is not differentiable, since the closest point $q^* \in \mathcal{M}_i$ to the robot i could be switched discontinuously. Therefore, the theoretical analysis is based on the generalized gradient of $\mathcal{H}(V)$, which is derived in this section.

The generalized gradient of $f : \mathbb{R}^N \to \mathbb{R}$ at x is defined as

$$\partial f(x) := \{\zeta \in \mathbb{R}^N \,|\, f^o(x; v) \geq v \cdot \zeta, \forall v \in \mathbb{R}^N\} \tag{23}$$

where

$$f^o(x; v) := \limsup_{\substack{y \to x \\ h \to 0+}} \frac{f(y + hv) - f(y)}{h}. \tag{24}$$

is the generalized directional derivative of f at x in the direction of $v \in \mathbb{R}^N$. A function $f : \mathbb{R}^N \to \mathbb{R}$ is said to be regular at $x \in \mathbb{R}^N$, if the right directional derivative

$$f'(x; v) := \lim_{h \to 0+} \frac{f(x + hv) - f(x)}{h} \tag{25}$$

exists, and $f^o(x; v) = f'(x; v)$ for all $v \in \mathbb{R}^N$.

In order to derive the generalized gradient of $\mathcal{H}(V)$, we first rewrite H_i in (17) as

$$H_i(V) = \min \left\{ \min_{j \in \{1,\ldots,n\} \setminus \{i\}} F_{(i,j)}, \min_{e \in \mathrm{Ed}(\mathcal{P})} G_{(i,e)} \right\} \tag{26}$$

without using $\mathcal{N}_i$. Then, we use the following fact.

Proposition 2: If $q_i \neq q_j$ and $q_i \in \mathrm{int}(\mathcal{P})$, then the functions $F_{(i,j)}(V)$ and $G_{(i,e)}(V)$ are continuously differentiable for each $(i, j) \in \mathcal{IJ}$ and $(i, e) \in \mathcal{IE}$, where

$$\mathcal{IJ} := \{(i, j) \mid i \in \{1, \ldots, n\}, j \in \{1, \ldots, n\}, i \neq j\}$$
$$\mathcal{IE} := \{(i, e) \mid i \in \{1, \ldots, n\}, e \in \mathrm{Ed}(\mathcal{P})\}$$

and $\mathrm{int}(S)$ denotes the interior of a set S.

Proof: See Appendix D. ∎

Since Proposition 2 implies that $-F_{(i,j)}$ and $-G_{(i,e)}$ are continuously differentiable, they are locally Lipschitz and regular [27]. Thus, we obtain

$$\begin{aligned} \partial H_i(V) = \ & \mathrm{co}(\{\nabla F_{(i,j)}(V) \mid F_{(i,j)} = H_i\} \\ & \cup \{\nabla G_{(i,e)}(V) \mid G_{(i,e)} = H_i\}) \end{aligned} \tag{27}$$

by applying Proposition 5 in Appendix E-1 to

$$-H_i(V) = \max \left\{ \max_{j \in \{1,\ldots,n\} \setminus \{i\}} -F_{(i,j)}, \max_{e \in \mathrm{Ed}(\mathcal{P})} -G_{(i,e)} \right\}.$$

Further, by applying Proposition 5 to

$$-\mathcal{H}(V) = \max_{i \in \{1,\ldots,n\}} -H_i(V) \tag{28}$$

it is seen that $-\mathcal{H}(V)$ is regular and that

$$\partial \mathcal{H}(V) = \mathrm{co}\{\partial H_i(V) \mid i \in I_H(V)\} \tag{29}$$

where $I_H(V) := \{i \in \{1, \ldots, n\} \mid H_i(V) = \mathcal{H}(V)\}$. By substituting (27) into (29), the generalized gradient of $\partial \mathcal{H}$ is written as

$$\begin{aligned} \partial \mathcal{H}(V) = \ & \mathrm{co}(\{\nabla F_{(i,j)}(V) \mid (i, j) \in I_F(V)\} \\ & \cup \{\nabla G_{(i,e)}(V) \mid (i, e) \in I_G(V)\}) \end{aligned} \tag{30}$$

where

$$\begin{aligned} I_F(V) &:= \{(i, j) \in \mathcal{IJ} \mid F_{(i,j)}(V) = \mathcal{H}(V)\} \\ I_G(V) &:= \{(i, e) \in \mathcal{IE} \mid G_{(i,e)}(V) = \mathcal{H}(V)\}. \end{aligned} \tag{31}$$

B. Case of Fixed and Nonconvex Formation

In this section, we consider the case where the polygonal region $\mathcal{P}$ is fixed. In such cases, we have $u_{mi} = 0_2$ $(i = 1, \ldots, n)$, since $\dot{\sigma} = 0_2, \dot{\theta} = 0_m$, and $\dot{p}_0 = 0_2$. Thus, the overall system of n robots is described in a vector form as

$$\dot{Q} = U_s, \quad U_s := [u_{s1}^T, \ldots, u_{sn}^T]^T \tag{32}$$

which is equivalently

$$\dot{V} = \mathcal{U}_s, \quad \mathcal{U}_s := [U_s^T, 0_{m+4}^T]^T. \tag{33}$$

Due to the nonsmoothness of u_s, it is not straightforward to show that $\mathcal{H}$ is not decreasing, even in cases where $\mathcal{P}$ is fixed. One possible way to show this is to apply the nonsmooth Lyapunov theory [28], [29] based on the Filipov solution to nonsmooth dynamical systems [30], by regarding $\mathcal{H}$ as a nonsmooth Lyapunov function. However, it is difficult to show that each element of the set-valued Lie derivative of $\mathcal{H}$ along the Filipov solution is nonnegative even in cases where $\mathcal{P}$ is a convex region, since the control law in (14) is decentralized in the sense that only the information on the closest point q^* from each robot is used. This topic is discussed in [26] based on the property that each element in the set-valued Lie derivative of $\mathcal{H}$ with respect to U_s is equivalent to $\zeta \cdot U_s$ for any $\zeta \in \partial\mathcal{H}$. However, it is uncertain whether this property holds except for the case where the set $\mathrm{argmin}_{q \in \mathcal{M}_i} \|q_i - q\|$ of the closest point q^* in (15) is a singleton. Thus, unlike these existing studies, we show that $\mathcal{H}(V)$ is not decreasing if the zero-order hold control is applied for a sufficiently short sampling period Δt. It is reasonable to focus on the zero-order hold control, since it is used in many practical cases.

From (33), it holds that $V(t + \Delta t) = V(t) + \mathcal{U}_s(t)\Delta t$, when $\mathcal{U}_s(t)$ is applied for the period $[t, t + \Delta t]$. Thus, we aim to show that $\mathcal{H}(V(t) + \mathcal{U}_s\Delta t)$ is not larger than $\mathcal{H}(V(t))$ as follows.

Theorem 1: For each V, which satisfies $q_i \neq q_j$ and $q_i \in \mathrm{int}(\mathcal{P})$, there exists $T > 0$ such that

$$\mathcal{H}(V + \mathcal{U}_s\Delta t) - \mathcal{H}(V) \geq 0, \quad \forall \Delta t \in (0, T). \tag{34}$$

Furthermore, if $u_{si} \neq 0$ for any $i \in I_H(V)$, there exists $T > 0$ such that

$$\mathcal{H}(V + \mathcal{U}_s\Delta t) - \mathcal{H}(V) > 0, \quad \forall \Delta t \in (0, T). \tag{35}$$

Proof: We first show the second part of the theorem. As mentioned in Section IV-A, $-\mathcal{H}(V)$ is regular. Further, $-\mathcal{H}$ is locally Lipschitz near V, since $-F_{(i,j)}(V)$ and $-G_{(i,e)}(V)$ are each locally Lipschitz near V for $(i, j) \in \mathcal{IJ}$ and $(i, e) \in \mathcal{IE}$ [27]. Thus, the directional derivative of $\mathcal{H}$ in the direction of $\mathcal{U}_s$ is written as

$$\mathcal{H}'(V; \mathcal{U}_s) = \min\{\zeta \cdot \mathcal{U}_s \mid \zeta \in \partial\mathcal{H}(V)\} \tag{36}$$

according to Lemma 1 in Appendix E-2. Since it holds that $\min\{\zeta \cdot \mathcal{U}_s \mid \zeta \in \partial\mathcal{H}(V)\} \geq \frac{1}{K} \min_{i \in I_H(V)} \|u_{si}\|^2$ from Lemma 3, we have $\mathcal{H}'(V; \mathcal{U}_s) \geq \frac{1}{K} \min_{i \in I_H(V)} \|u_{si}\|^2$. For the right directional derivative of $g(\epsilon) := \mathcal{H}(V + \epsilon\mathcal{U}_s) - \mathcal{H}(V)$, we obtain

$$\begin{aligned} g'_+(0) &:= \lim_{h \to 0+} \frac{g(0+h) - g(0)}{h} = \lim_{h \to 0+} \frac{\mathcal{H}(V + h\mathcal{U}_s) - \mathcal{H}(V)}{h} \\ &= \mathcal{H}'(V; \mathcal{U}_s) \geq \frac{1}{\hat{K}} \min_{i \in I_H(V)} \|u_{si}\|^2 > 0 \end{aligned} \tag{37}$$

due to the assumption that $u_{si} \neq 0$ for any $i \in I_H(V)$. Therefore, since $g(0) = 0$ and $g'_+(0) > 0$, it holds that $g(\epsilon) > 0$ for a sufficiently small $\epsilon > 0$, which concludes the second part of Theorem 1.

Next, we show the first part. It holds from Lemma 6 that

$$\begin{aligned} g'_+(\epsilon) &= \lim_{h \to 0+} \frac{g(\epsilon + h) - g(\epsilon)}{h} \\ &= \lim_{h \to 0+} \frac{\mathcal{H}(V + \epsilon\mathcal{U}_s + h\mathcal{U}_s) - \mathcal{H}(V + \epsilon\mathcal{U}_s)}{h} \\ &= \mathcal{H}'(V + \epsilon\mathcal{U}_s; \mathcal{U}_s) \\ &= \min\{\zeta \cdot \mathcal{U}_s \mid \zeta \in \partial\mathcal{H}(V + \epsilon\mathcal{U}_s)\} \geq 0, \quad \forall \epsilon \in (0, T) \end{aligned} \tag{38}$$

for some $T > 0$. Since $\mathcal{H}$ is locally Lipschitz, g is also locally Lipschitz. Thus from Theorem 3 in Appendix E-1, there exists $\epsilon^* \in (0, \epsilon)$ such that $g(\epsilon) \in \{\xi\epsilon \mid \xi \in \partial g(\epsilon^*)\}$. Now, let Ω_g denote the set of points in $\mathbb{R}^2$ at which g is not differentiable. If ϵ_k $(k = 1, 2, \ldots)$ denotes the sequence which satisfies that $\epsilon_k \to \epsilon^* (\mathrm{as}\, k \to \infty)$ and $\epsilon_k \notin \Omega_g (\forall k)$, the derivative at ϵ_k can be obtained as $g'(\epsilon_k) = g'_+(\epsilon_k)$. Furthermore, it is seen from (38) that $g'_+(\epsilon_k) \geq 0$ for a sufficiently large k, which implies $\lim_{k \to \infty} g'(\epsilon_k) \geq 0$. Therefore, since it holds from Theorem 4 that

$$\partial g(\epsilon^*) = \mathrm{co}\left\{ \lim_{k \to +\infty} g'(\epsilon_k) \mid \epsilon_k \to \epsilon^*, \epsilon_k \notin \Omega_g \right\} \tag{39}$$

we have $\xi \geq 0$ for any $\xi \in \partial g(\epsilon^*)$. Thus, $g(\epsilon) \geq 0, \forall \epsilon \in (0, T)$, since $g(\epsilon) \in \{\xi\epsilon \mid \xi \in \partial g(\epsilon^*)\}$. ■

C. Case of Variable Formation

In cases where (σ, θ, p_0) is variable, the cost function $\mathcal{H}(V)$ is not necessarily nondecreasing, even if the locational optimization algorithm in Section III-B is used. Therefore, we aim to guarantee that the input for the subtask u_{si} $(i = 1, \ldots, n)$ makes the value of $\mathcal{H}(V)$ greater than that in the case without u_{si}. If this is guaranteed, the disposition of the robots is improved in terms of both the collision avoidance and the formation shape control, since $\mathcal{H}(V)$ takes into account the distance between a robot and a boundary of the polygon, as well as the distance between robots. The property $\mathcal{H}(V) > 0$, which is achieved without u_{si} $(i = 1, \ldots, n)$ in Section III-A, is also achieved when u_{si} is applied in addition to u_{mi}. Thus, in particular, $q_i \in \mathcal{P}$ $(i = 1, \ldots, n)$ is also achieved at $t > 0$, if it is initially achieved at $t = 0$.

The overall system of n robots is described as

$$\begin{aligned} &\dot{V} = \mathcal{U} = \mathcal{U}_m + \mathcal{U}_s \\ &\mathcal{U} := [u_1^T, \ldots, u_n^T, \dot{\sigma}^T, \dot{\theta}^T, \dot{p}_0^T]^T \\ &\mathcal{U}_m := [u_{m1}^T, \ldots, u_{mn}^T, \dot{\sigma}^T, \dot{\theta}^T, \dot{p}_0^T]^T. \end{aligned} \tag{40}$$

Similarly in Section IV-B, we consider the situation where the zero-order hold control is applied to (40) for a sufficiently short sampling period Δt. In other words, $(\mathcal{U}, \mathcal{U}_m, \mathcal{U}_s)$ is fixed during the period Δt. This implies in particular that the number of links M, i.e., the dimension of θ is also fixed during the period Δt. In such a case, it holds from (40) that $V(t+\Delta t) = V(t) + \mathcal{U}(t)\Delta t$, when $\mathcal{U}(t)$ is applied for the period $[t, t+\Delta t]$. Likewise, we have $V(t+\Delta t) = V(t) + \mathcal{U}_m(t)\Delta t$, if $\mathcal{U}(t) = \mathcal{U}_m(t)$ is applied for the period $[t, t+\Delta t]$. Thus, we compare the values of $\mathcal{H}(V(t) + \mathcal{U}(t)\Delta t)$ and $\mathcal{H}(V(t) + \mathcal{U}_m(t)\Delta t)$ in the following theorem.

Theorem 2: For each V that satisfies $q_i \neq q_j$ and $q_i \in \mathrm{int}(\mathcal{P})$, there exists $T > 0$ such that

$$\mathcal{H}(V + \mathcal{U}\Delta t) > \mathcal{H}(V + \mathcal{U}_m \Delta t), \quad \forall \Delta t \in (0, T) \tag{41}$$

if $u_{si} \neq 0$ for any $i \in I_H(V)$.

Proof: From Lemma 1, we have

$$\mathcal{H}'(V; \mathcal{U}) = \min_{\zeta \in \partial \mathcal{H}(V)} \zeta \cdot \mathcal{U}, \quad \mathcal{H}'(V; \mathcal{U}_m) = \min_{\zeta \in \partial \mathcal{H}(V)} \zeta \cdot \mathcal{U}_m.$$

From $\zeta \cdot \mathcal{U} = \zeta \cdot (\mathcal{U}_m + \mathcal{U}_s)$, we obtain

$$\min_{\zeta \in \partial \mathcal{H}(V)} \zeta \cdot \mathcal{U} \geq \min_{\zeta \in \partial \mathcal{H}(V)} \zeta \cdot \mathcal{U}_m + \min_{\zeta \in \partial \mathcal{H}(V)} \zeta \cdot \mathcal{U}_s. \tag{42}$$

This implies

$$\mathcal{H}'(V; \mathcal{U}) - \mathcal{H}'(V; \mathcal{U}_m) \geq \min_{\zeta \in \partial \mathcal{H}(V)} \zeta \cdot \mathcal{U}_s. \tag{43}$$

From Lemma 3, we have

$$\zeta \cdot \mathcal{U}_s \geq \frac{1}{\hat{K}} \min_{i \in I_H(V)} \|u_{si}\|^2, \quad \forall \zeta \in \partial \mathcal{H}(V). \tag{44}$$

It follows from (43) and (44) that

$$\mathcal{H}'(V; \mathcal{U}) - \mathcal{H}'(V; \mathcal{U}_m) \geq \frac{1}{\hat{K}} \min_{i \in I_H(V)} \|u_{si}\|^2. \tag{45}$$

From the definition of $\mathcal{H}'(V; \mathcal{U})$ and $\mathcal{H}'(V; \mathcal{U}_m)$, (45) implies

$$\lim_{h \to 0+} \frac{\mathcal{H}(V + h\mathcal{U}) - \mathcal{H}(V + h\mathcal{U}_m)}{h} \geq \frac{1}{\hat{K}} \min_{i \in I_H(V)} \|u_{si}\|^2. \tag{46}$$

Thus, if $u_{si} \neq 0$ for any $i \in I_H(V)$, we have

$$\lim_{h \to 0+} \frac{\mathcal{H}(V + h\mathcal{U}) - \mathcal{H}(V + h\mathcal{U}_m)}{h} > 0. \tag{47}$$

Therefore, there exists T that satisfies (41). ■

In the case of variable formations, it is difficult to obtain a result corresponding to the first part in Theorem 1. Namely, it is difficult to show that there exits T such that $\mathcal{H}(V + \mathcal{U}\Delta t) \geq \mathcal{H}(V + \mathcal{U}_m \Delta t)$ for any $\Delta t \in (0, T)$, in the case where $u_{si} = 0$ for some $i \in I_H(V)$. One reason for the difficulty is that even if $\lim_{h \to 0+} [\mathcal{H}(V + h\mathcal{U}) - \mathcal{H}(V + h\mathcal{U}_m)] \geq 0$, which can be easily shown from (46), we cannot guarantee $\mathcal{H}(V + h\mathcal{U}) \geq \mathcal{H}(V + h\mathcal{U}_m)$ for any $h \in (0, T)$. In other words, if $\lim_{h \to 0+} [\mathcal{H}(V + h\mathcal{U}) - \mathcal{H}(V + h\mathcal{U}_m)] = 0$, then there could be some $h \in (0, T)$ that violates $\mathcal{H}(V + h\mathcal{U}) \geq \mathcal{H}(V + h\mathcal{U}_m)$, even if an arbitrary small T is chosen. However, the control input u_{si} $(i = 1, \ldots, n)$ for the subtask rarely becomes 0 in the transient state of (σ, θ, p_0) where $u_{mi} \neq 0$, since the distances between robots or the the distances between a robot and a boundary of $\mathcal{P}$ are dynamically changing. On the other hand, in the steady state of (σ, θ, p_0) where $u_{mi} = 0$, it is proved by Theorem 1 that $\mathcal{H}(V)$ is not increased by u_{si}.

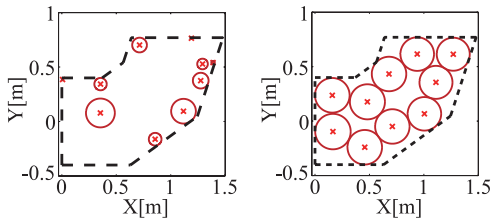

Fig. 5. Initial (left) and final (right) robot positions in Section V-A.

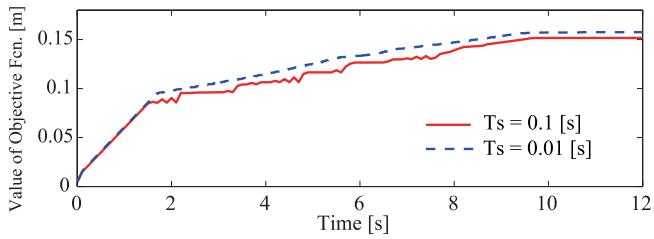

Fig. 6. Time response of $\mathcal{H}$ in the simulation of Section V-A.

V. Simulations

A. Fixed Nonconvex Formation

For a nonconvex polygon as shown in the dashed line in Fig. 5, the control input u_s for the subtask is applied using the zero-order hold with sampling time $T_s = 0.1$ and 0.01 s. The gain of the control law in (14) is $\hat{K} = 0.1$. We randomly generate 100 sets of initial positions of ten robots, and test whether the objective function $\mathcal{H}$ is nondecreasing or not. To this end, we compute the difference in $\mathcal{H}$ for each sampling interval and focus on the worst case in the sense that the largest decrease in $\mathcal{H}$ for a sampling interval $T_s = 0.1$ is observed. The initial positions of the robots in this case are shown by "×" in Fig. 5 (left), while the terminal positions in the case of $T_s = 0.1$ are shown in Fig. 5 (right). Note that the radius of the circle around each robot is equivalent to the value of H_i in (7). Thus, the minimum radius of the circles is the value of the objective function $\mathcal{H}$. The time response of $\mathcal{H}$ is shown in Fig. 6. Although it is shown in Theorem 1 that $\mathcal{H}$ is nondecreasing for a sufficiently small sampling interval, $\mathcal{H}$ is not rigorously nondecreasing in the simulation results of $T_s = 0.1$ and 0.01 s.

The solid and the dashed lines in Fig. 6 show the time responses of $\mathcal{H}$ for $T_s = 0.1$ and 0.01, respectively, from the same initial positions in Fig. 5 (left). The decrease in $\mathcal{H}$ is negligible for $T_s = 0.01$, where the largest decrease for sampling intervals is about 5.0×10^{-4}. On the other hand, the graph in $\mathcal{H}$ is more oscillatory for $T_s = 0.1$, where the largest decrease is about 5.0×10^{-3}. Nevertheless, $\mathcal{H}$ successfully grows to a value similar to that in the case of $T_s = 0.01$.

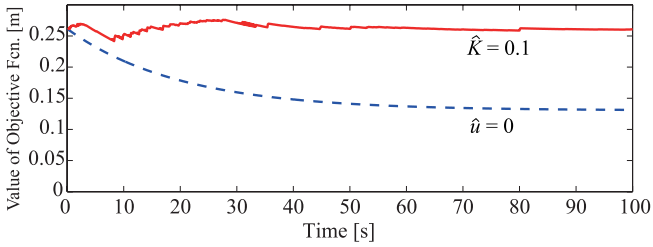

Fig. 7. Time response of $\mathcal{H}$ for the simulation in Section V-B.

B. Variable Rectangular Formation

We consider a variable rectangular formation with $\dot{\sigma}_1 > 0$ and $\dot{\sigma}_2 < 0$, in the same way as in Example 1. The value of σ is changed with $\dot{\sigma}_1 = K_1(\sigma_{d1} - \sigma_1)$ and $\dot{\sigma}_2 = K_2(\sigma_{d2} - \sigma_2)$, where $K_1 = K_2 = 0.05$. The target value of σ is $\sigma_d = [8, 2]^T$, while the initial value is $\sigma(0) = [4, 4]^T$.

To test the influence of the change in σ on $\mathcal{H}$, the initial positions of 50 robots are generated by applying the control law for the initial rectangle until $\mathcal{H}$ converges from randomly selected initial positions. As a result, $\mathcal{H}$ is not changed from the initial value, unless σ changes. From such simulations for 100 different sets of initial positions, we focus on the worst case, in the sense that the largest decrease from the initial value of $\mathcal{H}$ is observed for $\hat{K} = 0.1$. The time response of $\mathcal{H}$ in this case is shown in the solid line in Fig. 7. The largest decrease from the initial value is about 1.9×10^{-2} m. On the other hand, as shown in the dashed line, the value of $\mathcal{H}$ is monotonically decreased to about half of the initial value if the control input for the subtask is not applied. See also the multimedia component for an animation of the positions of the robots.

C. Bending Formation

For the rectangular formation of $\sigma = [8, 2]^T$ obtained in Section V-B to make a turn in the narrow corner as shown in Fig. 8, $\dot{p}_0$ and $\dot{\theta}_0$ are given as follows:

$$\dot{p}_0(t) = \begin{cases} \begin{bmatrix} -v_1 \\ 0 \end{bmatrix}, & \text{if } 0 \le t < t_1 \\ \begin{bmatrix} -v_2 \sin \omega t \\ -v_2 \cos \omega t \end{bmatrix}, & \text{if } t_1 \le t < t_1 + t_2 \\ \begin{bmatrix} 0 \\ v_1 \end{bmatrix}, & \text{if } t_1 + t_2 \le t \end{cases}$$

$$\dot{\theta}_0(t) = \begin{cases} 0, & \text{if } 0 \le t < t_1 \\ -\omega, & \text{if } t_1 \le t < t_1 + t_2 \\ 0, & \text{if } t_1 + t_2 \le t \end{cases} \tag{48}$$

where $v_1 = 0.1, v_2 = 0.05, \omega = v_2/1.4, t_1 = 5$ and $t_2 = \pi/2\omega$. Thus, p_0 and θ_0 can be obtained from the initial values $p_0(0) = [0, 0]^T$ and $\theta_0(0) = 0$. Then, $\dot{\theta}_k$ $(k = 1, \ldots, m-1)$ is determined by using the method in [24], where $m = \sigma_1/L$, and $L = 0.5$ m.

We use 100 sets of initial positions of the robots, which are obtained as the final positions in the 100 cases in Section V-B, and focus on the worst case, in the sense that the largest decrease from the initial value of $\mathcal{H}$ is observed for $\hat{K} = 0.1$.

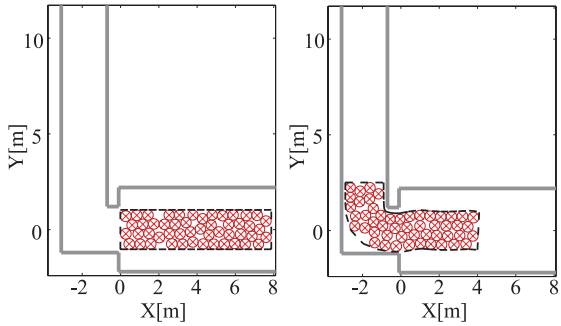

Fig. 8. Formation in a narrow corner at $t = 0$ (left) and $t = 60$ (right).

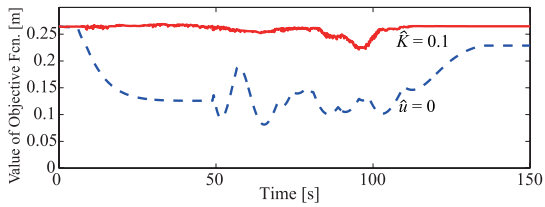

Fig. 9. Time response of $\mathcal{H}$ for the simulation in Section V-C.

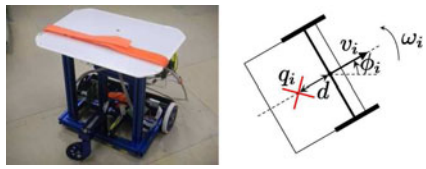

Fig. 10. Photograph (left) and schematic (right) of a robot used in the experiments.

The positions of the robots at $t = 0$ and $t = 60$ in this case are shown by "$\times$" in Fig. 8. An animation of the positions is included in the multimedia component. The time response of $\mathcal{H}$ is shown by the solid line in Fig. 9. The largest decrease from the initial value is about 2.8×10^{-2} m. On the other hand, if the control input u_s for the subtask is not applied, the value of $\mathcal{H}$ is decreased much more significantly, as shown in the dashed line, since the distances between robots become small inside the corner.

VI. Experiments

The proposed formation control method is applied to a group of eight robots. For each robot, we use a mobile robot platform "beego" (Techno Craft), which is a two-wheeled skid-steer robot with one caster wheel, as shown in Fig. 10 (left). See also the multimedia component for movies showing experiments in this section.

The model of this robot is described as follows:

$$\begin{bmatrix} \dot{X}_i \\ \dot{Y}_i \\ \dot{\phi}_i \end{bmatrix} = \begin{bmatrix} \cos\phi_i & 0 \\ \sin\phi_i & 0 \\ 0 & 1 \end{bmatrix} \begin{bmatrix} v_i \\ \omega_i \end{bmatrix}, \quad i = 1, \ldots, 8 \tag{49}$$

where (X_i, Y_i) denotes the position of the center of the axle, and ϕ_i is the orientation of the robot i. The control inputs of this system are the translational and angular velocities (v_i, ω_i). To obtain the model as in (1) for this system, we define q_i as the

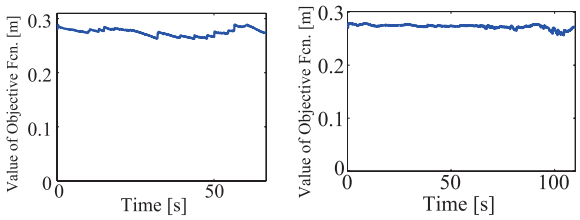

Fig. 11. Time responses of $\mathcal{H}$ for the experiments in Section VI-A (left) and B (right).

point with an offset $d = 0.1$ m from the center of the axle, as shown in Fig. 10 (right). Since we obtain

$$\dot{q}_i = B_i \begin{bmatrix} v_i \\ \omega_i \end{bmatrix} = u_i, \quad B_i := \begin{bmatrix} \cos\phi_i & d\sin\phi_i \\ \sin\phi_i & -d\cos\phi_i \end{bmatrix} \tag{50}$$

from (49), the input u_i, which is determined from the control algorithm, can be transformed to (v_i, ω_i) and applied to the real robot. The position and orientation of the vehicle are measured by dead reckoning.

A. Variable Rectangular Formation

In the same way as in Section V-B, we consider a variable rectangular formation. The target value of σ is $\sigma_d = [3.2, 1.0]^T$, while the initial value is $\sigma(0) = [1.6, 2.0]^T$. The values of the feedback gains K_1, K_2, and $\hat{K}$ are the same as in Section V-B. To choose the initial positions of the robots, we perform a simulation in which the control law is applied to the fixed rectangle of $\sigma = [1.6, 2.0]^T$ until $\mathcal{H}$ converges from a set of randomly selected initial positions of the robots. Based on the simulation result, we choose the initial positions as follows:

$$q_1 = \begin{bmatrix} 0.3 \\ 0.7 \end{bmatrix}, \quad q_2 = \begin{bmatrix} 0.3 \\ -0.15 \end{bmatrix}, \quad q_3 = \begin{bmatrix} 0.4 \\ -0.7 \end{bmatrix}, \quad q_4 = \begin{bmatrix} 0.7 \\ 0.3 \end{bmatrix}$$

$$q_5 = \begin{bmatrix} 0.9 \\ -0.3 \end{bmatrix}, \quad q_6 = \begin{bmatrix} 1.2 \\ 0.7 \end{bmatrix}, \quad q_7 = \begin{bmatrix} 1.3 \\ 0.1 \end{bmatrix}, \quad q_8 = \begin{bmatrix} 1.3 \\ -0.7 \end{bmatrix}.$$

Fig 11 (left) shows that the decrease in the value of $\mathcal{H}$ during the formation change is kept small. The largest decrease from the initial value is about 1.7×10^{-2} m.

B. Bending Formation

From the initial rectangular formation with $\sigma_d = [3.2, 1.0]^T$, a group of robots makes a turn by giving $\dot{p}_0$ and $\dot{\theta}_0$ in (48), where $v_1 = 0.05, v_2 = 0.025, \omega = v_2/0.96, t_1 = 3.9$, and $t_2 = \pi/2\omega$. The initial values of p_0 and θ_0 are $[0, 0]^T$ and 0, respectively. To choose the initial positions of the robots, we perform a simulation in which the control law is applied to the fixed rectangle of $\sigma = [3.2, 1.0]^T$ until $\mathcal{H}$ converges from a set of randomly selected initial positions of the robots. Based on the simulation result, we choose the initial positions as follows:

$$q_1 = \begin{bmatrix} 0.30 \\ -0.21 \end{bmatrix}, \quad q_2 = \begin{bmatrix} 0.70 \\ 0.22 \end{bmatrix}, \quad q_3 = \begin{bmatrix} 1.06 \\ -0.23 \end{bmatrix}, \quad q_4 = \begin{bmatrix} 1.41 \\ 0.23 \end{bmatrix}$$

$$q_5 = \begin{bmatrix} 1.76 \\ -0.23 \end{bmatrix}, \quad q_6 = \begin{bmatrix} 2.11 \\ 0.23 \end{bmatrix}, \quad q_7 = \begin{bmatrix} 2.47 \\ -0.23 \end{bmatrix}, \quad q_8 = \begin{bmatrix} 2.86 \\ 0.21 \end{bmatrix}.$$

Fig 11 (right) shows that the decrease in the value of $\mathcal{H}$ during the formation change is kept small. The largest decrease from the initial value is about 1.4×10^{-2} m.

VII. Conclusion

In this paper, we have presented a new method of controlling a group of mobile robots based on formation abstraction. In rectangular formations, a deformable polygonal formation is used to go through narrow spaces without colliding with obstacles. Furthermore, the robots continuously try to optimize their positions to decrease the risk of collisions by integrating a decentralized locational optimization algorithm into formation control. We have shown that the objective function for the locational optimization does not decrease for fixed nonconvex polygonal formation shapes if the zero-order hold control is applied for a sufficiently short sampling period. Then for the variable rectangular formation, we have also shown that the locational optimization algorithm makes the value of the objective function greater than the value in the case without the locational optimization. The effectiveness of the proposed method has been demonstrated in both simulations and real robot experiments. However, more studies are necessary in the future for an actual implementation. Since it is inevitable that the objective function is not necessarily nondecreasing in variable formation cases, robots need to have some margins in distances from other robots and from the boundary of the polygonal region in order to achieve two goals, i.e., maintaining robots in the region and avoiding collisions, which often conflict with each other. To this end, an important problem is how to determine the area of the polygonal region. It is also important to determine the speed of deformation appropriately, since the numbers of margins required depend on the speed of deformation. Emergency mechanisms, which change the priorities of two goals in the case where one of the two goals has to be given up to achieve, also need to be studied. In addition, although we assume that parameters such as L and σ_d are given in this paper, the algorithm to decide them on the basis of information on the environments should be studied in the future. Further theoretical studies are also required, since the theoretical analysis in this paper considers limited cases where the control law is implemented by using the zero-order hold control.

Appendix A
Front-unit Following Control

Front-unit following control methods [24], [25] aim to determine θ_k $(k = 1, \ldots, m-1)$ such that the joint positions p_{k+1} $(k = 1, \ldots, m-1)$ track the path of the first joint position p_1. To illustrate the basic idea behind these methods, we first assume that the joint positions p_{k+1} $(k = 1, \ldots, m-1)$ are initially on the target path at $t = 0$. Under this assumption, path tracking is accomplished at each time $t \geq 0$, if the velocity of each joint is always generated in the tangential direction of the target path. Let ψ_k $(k = 1, \ldots, m)$ denote the orientation of the tangent vector of the target path at the position p_k, as shown in Fig. 12. Then, the XY coordinate $(X_{p_{k+1}}, Y_{p_{k+1}})$ of p_{k+1} $(k = 1, \ldots, m-1)$

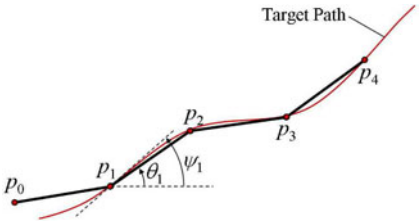

Fig. 12. Serial link and the target path ($m = 4$).

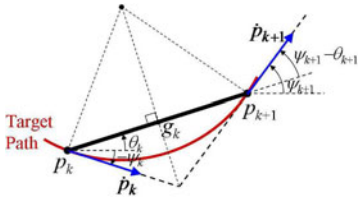

Fig. 13. Velocity of a link.

needs to satisfy

$$\dot{X}_{p_{k+1}} \sin\psi_{k+1} - \dot{Y}_{p_{k+1}} \cos\psi_{k+1} = 0. \tag{51}$$

From (51) and

$$\begin{aligned} \dot{X}_{p_{k+1}} &= \dot{X}_{p_k} - L\dot{\theta}_k \sin\theta_k \\ \dot{Y}_{p_{k+1}} &= \dot{Y}_{p_k} + L\dot{\theta}_k \cos\theta_k, \quad k = 0, \ldots, m-1 \end{aligned} \tag{52}$$

we obtain

$$\dot{\theta}_k = \frac{\dot{X}_{p_k} \sin\psi_{k+1} - \dot{Y}_{p_k} \cos\psi_{k+1}}{L\cos(\theta_k - \psi_{k+1})} \tag{53}$$

for $k = 1, \ldots, m-1$.

To estimate ψ_{k+1} $(k = 1, \ldots, m-1)$ in (53), the method in [25] stores the samples of (p_1, ψ_1) every time when the first joint proceeds a prescribed distance along the path. Note that ψ_1 is obtained from $\dot{p}_0$ and $\dot{\theta}_0$ as

$$\psi_1 = \tan^{-1}\frac{\dot{Y}_{p_1}}{\dot{X}_{p_1}} = \tan^{-1}\frac{\dot{Y}_{p_0} + L\dot{\theta}_0\cos\theta_0}{\dot{X}_{p_0} - L\dot{\theta}_0\sin\theta_0}. \tag{54}$$

The sample (p_1, ψ_1), which has the closest p_1 to p_{k+1} $(k = 1, \ldots, m-1)$ at the current time, is used to estimate ψ_{k+1}. Although (53) is derived under the assumption that joint positions p_{k+1} $(k = 1, \ldots, m-1)$ are initially on the target path, this assumption is not necessarily satisfied. Thus, joint positions are often off the target path. Therefore, the method in [25] estimates the tangent vector ψ_{k+1} at the orthogonal projection of p_{k+1} $(k = 1, \ldots, m-1)$ to the target path, and an additional feedback term is added in (53) to decrease the error between p_{k+1} $(k = 1, \ldots, m-1)$ and the target path.

On the other hand, [24] uses a simpler method which is based on an additional assumption that the transition rate of curvature of the target path is sufficiently small between two consecutive joints. In such cases, it is satisfied that

$$\psi_{k+1} - \theta_k = \theta_k - \psi_k, \quad k = 1, \ldots, m-1 \tag{55}$$

since the directions of $\dot{p}_{k+1}$ and $\dot{p}_k$ are symmetric with respect to the link k, as shown in Fig. 13. By using (51) and (55), we can simplify (53) as

$$\dot{\theta}_k = \frac{2(\dot{X}_{p_k}\sin\psi_k - \dot{Y}_{p_k}\cos\psi_k)}{L}. \tag{56}$$

Since (56) is also based on the assumptions which are not always satisfied, the joint positions p_{k+1} $(k = 1, \ldots, m-1)$ are often off the target path. Although the method in [24] is not able to handle the off tracking in general situations, it is proved that the tracking error converges to 0 in cases where the curvature of the target path is constant, under the assumptions in (3) and (4).

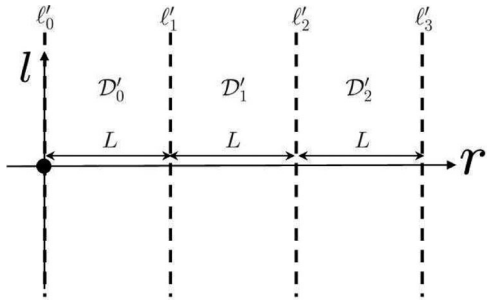

Fig. 14. r–l frame and region $\mathcal{D}'_k$.

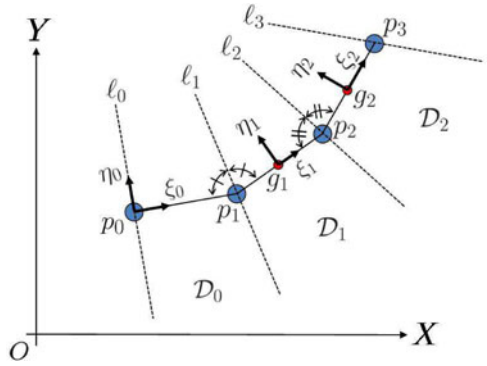

Fig. 15. ξ_k–η_k frame and region $\mathcal{D}_k$.

APPENDIX B
DETAILS ON TRANSFORMATION $T_{(p_0,\theta)}$

The transformation $T_{(p_0,\theta)}$ maps the absolute coordinate q to the r–l coordinate as shown in Fig. 14, whose origin corresponds to the front end point p_0 of the serial link structure in Fig. 15. Points on a link are mapped onto the r-axis. The line ℓ_k $(k = 0, \ldots, m)$ in Fig. 15 is mapped to ℓ'_k in Fig. 14. For $k = 1, \ldots, m-1$, the line ℓ_k is the bisector of the angle between two line segments connecting at p_k, while ℓ_0 and ℓ_m are perpendicular to the first and the last links, respectively. The line ℓ'_k $(k = 0, \ldots, m)$ is parallel to the l-axis and passes through the point $(kL, 0)$. Furthermore, the region $\mathcal{D}_k$ $(k = 0, \ldots, m-1)$ between ℓ_k and ℓ_{k+1} is mapped to $\mathcal{D}'_k$ between ℓ'_k and ℓ'_{k+1}.

To describe $\mathcal{D}_k$ more clearly, we define the local coordinate (ξ_k, η_k) for $k = 0, \ldots, m-1$, which is obtained from the

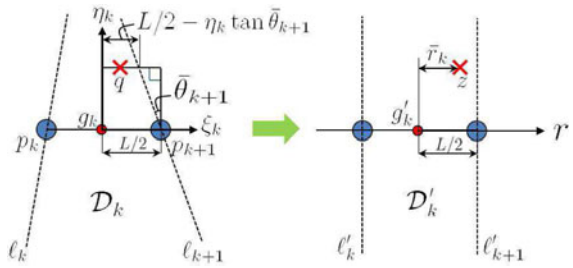

Fig. 16. Transformation from q to z.

absolute coordinate q, as follows:

$$\begin{bmatrix}\xi_k\\ \eta_k\end{bmatrix} = R^{-1}(\theta_k)(q-g_k),\quad R(\theta):=\begin{bmatrix}\cos\theta & -\sin\theta\\ \sin\theta & \cos\theta\end{bmatrix} \tag{57}$$

where $g_k=\frac{p_k+p_{k+1}}{2}$ $(k=1,2,\dots m-1)$, and $g_0=p_0$. As shown in Fig. 15, the origin of the ξ_k–η_k coordinate system is g_k, and the ξ_k-axis is along the $(k+1)$th link. Using (ξ_k,η_k), the region $\mathcal{D}_k$ is described as

$$\mathcal{D}_k:=\left\{(\xi_k,\eta_k)\,\middle|\,-\frac{L}{2}+\eta_k\tan\bar{\theta}_k<\xi_k\le\frac{L}{2}-\eta_{k+1}\tan\bar{\theta}_{k+1}\right\}$$
$$k=1,2,\dots,m-1$$
$$\mathcal{D}_0:=\left\{(\xi_0,\eta_0)\,\middle|\,0\le\xi_0\le L-\eta_1\tan\bar{\theta}_1\right\} \tag{58}$$

where $\bar{\theta}_k:=\frac{\theta_k-\theta_{k-1}}{2}$. If the local coordinate (ξ_k,η_k), which is transformed from the absolute coordinate q, satisfies $(\xi_k,\eta_k)\in\mathcal{D}_k$, the r–l coordinate is given as

$$r=\begin{cases}kL+\dfrac{L}{2}+\dfrac{L}{L-2\eta_k\tan\bar{\theta}_k^+}\xi_k, & \text{if } k\neq 0\\ \dfrac{L}{L-\eta_k\tan\bar{\theta}_{k+1}}\xi_k, & \text{if } k=0\end{cases}$$
$$l=\eta_k \tag{59}$$

where

$$\bar{\theta}_k^+=\begin{cases}\bar{\theta}_{k+1}, & \text{if } \xi_k\ge 0\\ \bar{\theta}_k, & \text{if } \xi_k<0.\end{cases} \tag{60}$$

Fig. 16 illustrates the case of $\xi_k\ge 0$ and $k\neq 0$. The middle point g_k of the link is mapped to $g'_k:=[kL+\frac{L}{2},0]^T$. Let $\bar{r}_k$ be the difference from g'_k to z in the r-direction, as shown in Fig. 16. Then, $z=[r,l]^T$ is determined such that $\xi_k:\frac{L}{2}-\eta_k\tan\bar{\theta}_{k+1}=\bar{r}_k:\frac{L}{2}$. Thus, in Fig. 16, the difference from g_k to q in the direction along the link is enlarged in the r–l frame by multiplying $\frac{L/2}{L/2-\eta_k\tan\bar{\theta}_{k+1}}$.

Appendix C

Details on the Control for the Main Task

Let $(\xi_{(k,i)},\eta_{(k,i)})$ be the $(\xi_k$–$\eta_k)$ coordinate of q_i for $i=1,\dots,n$ and $k=0,\dots,m-1$. We also define k_i as k, which satisfies $(\xi_{(k,i)},\eta_{(k,i)})\in\mathcal{D}_k$. Then, from (57), the relationship between q_i and $(\xi_{(k_i,i)},\eta_{(k_i,i)})$ is written as

$$q_i=g_{k_i}+R(\theta_{k_i})\begin{bmatrix}\xi_{(k_i,i)}\\ \eta_{(k_i,i)}\end{bmatrix}. \tag{61}$$

By differentiating (61), we obtain

$$\dot{q}_i=\dot{g}_{k_i}+\dot{\theta}_{k_i}R'(\theta_{k_i})\begin{bmatrix}\xi_{(k_i,i)}\\ \eta_{(k_i,i)}\end{bmatrix}+R(\theta_{k_i})\begin{bmatrix}\dot{\xi}_{(k_i,i)}\\ \dot{\eta}_{(k_i,i)}\end{bmatrix} \tag{62}$$

where

$$\dot{g}_{k_i}=\frac{\dot{p}_{k_i}+\dot{p}_{k_i+1}}{2},\quad R'(\theta):=\begin{bmatrix}-\sin\theta & -\cos\theta\\ \cos\theta & -\sin\theta\end{bmatrix}. \tag{63}$$

The relationship between z_i and $(\xi_{(k_i,i)},\eta_{(k_i,i)})$ is given from (59) as

$$\xi_{(k_i,i)}=\begin{cases}\dfrac{L-2l_i\tan\bar{\theta}_{k_i}^+}{L}\bar{r}_{k_i}, & \text{if } k_i\neq 0\\ \dfrac{L-l_i\tan\bar{\theta}_1}{L}r_i, & \text{if } k_i=0\end{cases}$$
$$\eta_{(k_i,i)}=l_i \tag{64}$$

where $\bar{r}_{k_i}:=r_i-k_iL-\frac{L}{2}(k_i=1,\dots,m-1)$. From (64), we obtain

$$\dot{\xi}_{(k_i,i)}=$$
$$\begin{cases}\dot{r}_i\dfrac{L-2l\tan\bar{\theta}_{k_i}^+}{L}-\dfrac{2\bar{r}_{k_i}}{L}\left(\dot{l}_i\tan\bar{\theta}_{k_i}^+ +\dfrac{l_i\dot{\bar{\theta}}_{k_i}^+}{\cos^2\bar{\theta}_{k_i}^+}\right), & \text{if } k_i\neq 0\\ \dot{r}_i\dfrac{L-l\tan\bar{\theta}_1}{L}-\dfrac{r_i}{L}\left(\dot{l}_i\tan\bar{\theta}_1+\dfrac{l_i\dot{\bar{\theta}}_1}{\cos^2\bar{\theta}_1}\right), & \text{if } k_i=0\end{cases}$$
$$\dot{\eta}_{(k_i,i)}=\dot{l}_i. \tag{65}$$

In order for $\dot{z}_i$ to satisfy (11), we substitute (11) into (65) and determine $u_i=u_{mi}$ in (1) as the right-hand side of (62).

The computation of u_{mi} is summarized as follows.

1) (p_0,θ,σ) at t is given from the central computer.
2) $(\xi_{(k,i)},\eta_{(k,i)})$ is computed for $k=0,\dots,m-1$ by substituting $q=q_i$ into (57).
3) k_i is determined as k, which satisfies $(\xi_{(k,i)},\eta_{(k,i)})\in\mathcal{D}_k$.
4) (r_i,l_i) is computed by substituting $k=k_i$ and $(\xi_k,\eta_k)=(\xi_{(k_i,i)},\eta_{(k_i,i)})$ into (59).
5) $(\dot{\xi}_{(k_i,i)},\dot{\eta}_{(k_i,i)})$ is obtained by substituting (11) into (65).
6) u_{mi} is given by computing the right-hand side of (62), where $\dot{p}_k$ $(k=1,\dots,m)$ and $\dot{\theta}_k$ $(k=1,\dots,m-1)$ are recursively computed by using (52) and (56) (or (53)).

Appendix D

Proof of Proposition 2

For $F_{(i,j)}(V)$, we have

$$\frac{\partial F_{(i,j)}}{\partial q_i}=\frac{1}{2}\frac{(q_i-q_j)^T}{\|q_i-q_j\|},\ \frac{\partial F_{(i,j)}}{\partial q_j}=\frac{1}{2}\frac{(q_j-q_i)^T}{\|q_i-q_j\|}. \tag{66}$$

Other elements of $\frac{\partial F_{(i,j)}}{\partial V}$ are 0. Thus, $F_{(i,j)}(V)$ is continuously differentiable, if $q_i\neq q_j$. For $G_{(i,j)}(V)$, we have

$$\frac{\partial G_{(i,j)}}{\partial q_i}=\frac{(q_i-\mathrm{Cp}_e(q_i))^T}{\|q_i-\mathrm{Cp}_e(q_i)\|}. \tag{67}$$

Other elements of $\frac{\partial G_{(i,j)}}{\partial Q}$ are 0. Since $\mathrm{Cp}_e(q_i)$ in (16) is continuous with respect to q_i, it is shown that $\frac{\partial G_{(i,j)}}{\partial q_i}$ in (67) is

continuous, if $q_i \in \mathrm{int}(\mathcal{P})$. Thus, we next show that $\frac{\partial G_{(i,j)}}{\partial V_2}$ exists and is continuous, where $V_2 := [\sigma^T, \theta^T, p_0^T]^T$. Each vertex ($v_R$ or v_L) of the edge e is one of the vertices of the polygon $\mathcal{P}$. The $2(m+1)$ vertices of $\mathcal{P}$ are located at

$$R(\theta_0)\begin{bmatrix} 0 \\ \pm\frac{\sigma_2}{2} \end{bmatrix} + p_0, \quad R(\theta_m)\begin{bmatrix} \sigma_1 - (m-1)L \\ \pm\frac{\sigma_2}{2} \end{bmatrix} + p_m$$

$$R(\theta_k)\begin{bmatrix} -\frac{L}{2} \pm \frac{\sigma_2}{2}\tan\bar{\theta}_k \\ \pm\frac{\sigma_2}{2} \end{bmatrix} + g_k, \quad k = 1, \ldots, m-1.$$

Note that $|\bar{\theta}_k| \leq \pi/4$ for $k = 1, \ldots, m-1$ since the joint angles are limited as in (4). Thus, $\frac{\partial v_R}{\partial V_2}$ and $\frac{\partial v_L}{\partial V_2}$ are continuous for each edge $e \in \mathrm{Ed}(\mathcal{P})$. This implies that $\frac{\partial G_{(i,e)}}{\partial V_2} = \frac{(q_i - \mathrm{Cp}_e)^T}{\|q_i - \mathrm{Cp}_e\|}\frac{\partial (q_i - \mathrm{Cp}_e)}{\partial V_2}$ is continuous, if q_i is not on the boundaries of D_M. We now show the continuity of $\frac{\partial G_{(i,e)}}{\partial V_2}$ on the boundary between D_L and D_M, that is, in the case where $(q_i - v_L)\cdot(v_R - v_L) = 0$. For $q_i \in D_L$, we have

$$\frac{\partial G_{(i,e)}}{\partial V_2} = \frac{(q_i - v_L)^T}{\|q_i - v_L\|}\frac{\partial (q_i - v_L)}{\partial V_2} = -\frac{(q_i - v_L)^T}{\|q_i - v_L\|}\frac{\partial v_L}{\partial V_2} \quad (68)$$

since $\mathrm{Cp}_e = v_L$. For $q_i \in D_M$, we have

$$\frac{\partial \mathrm{Cp}_e}{\partial V_2} = \frac{\partial v_L}{\partial V_2} + \frac{v_R - v_L}{\|v_R - v_L\|^2}\frac{\partial\{(q_i - v_L)\cdot(v_R - v_L)\}}{\partial V_2}$$

since $(q_i - v_L)\cdot(v_R - v_L) = 0$. This implies that

$$\frac{\partial G_{(i,e)}}{\partial V_2} = -\frac{(q_i - \mathrm{Cp}_e)^T}{\|q_i - \mathrm{Cp}_e\|}\frac{\partial \mathrm{Cp}_e}{\partial V_2} = -\frac{(q_i - v_L)^T}{\|q_i - v_L\|}\frac{\partial v_L}{\partial V_2} \quad (69)$$

since $(q_i - v_L)\cdot(v_R - v_L) = 0$. Therefore, it is seen from (68) and (69) that $\frac{\partial G_{(i,e)}}{\partial V_2}$ is continuous on the boundary between D_M and D_L. The continuity on the boundary between D_M and D_R can be shown in the same way, since $\mathrm{Cp}_e = v_R + \frac{(q_i - v_R)\cdot(v_R - v_L)}{\|v_R - v_L\|^2}(v_R - v_L)$ for $q_i \in D_M$. Thus, $\frac{\partial G_{(i,e)}}{\partial V_2}$ is continuous.

APPENDIX E
PRELIMINARY RESULTS TO PROVE THEOREMS 1 AND 2

1) Results From Nonsmooth Analysis [27]

The following proposition shows that the generalized directional derivative $f^o(x; v)$ can be written by using the generalized gradient ∂f.

Proposition 3: Let f be locally Lipschitz near x. Then, for every v in $\mathbb{R}^N$

$$f^o(x; v) = \max\{\zeta \cdot v \mid \zeta \in \partial f(x)\}. \quad (70)$$

Proof: See [27, Prop. 2.1.2(b)]. ∎

By using ∂f, the mean value theorem for locally Lipschitz functions is described as follows.

Theorem 3: For x and y in $\mathbb{R}^N$, let $[x, y]$ denote the closed line segment consisting of all points $\lambda x + (1-\lambda)y$ for $\lambda \in [0, 1]$, and (x, y) denotes the open line segment. If f is locally Lipschitz on an open set containing $[x, y]$, there exists $z \in (x, y)$ such that

$$f(y) - f(x) \in \{\zeta \cdot (y - x) \mid \zeta \in \partial f(z)\}.$$

Proof: See [27, Th. 2.3.7]. ∎

The following results make the calculation of ∂f easier.

Proposition 4: For any scalar c, we have

$$\partial(cf)(x) = c\partial f(x). \quad (71)$$

Proof: See [27, Prop. 2.3.1]. ∎

Theorem 4: Let f be locally Lipschitz near x, and Ω_f denotes the set of points in $\mathbb{R}^N$ at which f is not differentiable. Then, for any other set of measure zero defined as S, we have

$$\partial f(x) := \mathrm{co}\left\{\lim_{k\to+\infty} \nabla f(x_k) \mid x_k \to x, x_k \notin S \cup \Omega_f\right\}. \quad (72)$$

Proof: See [27, Th 2.5.1]. ∎

Proposition 5: Suppose that f_i $(i = 1, \ldots, N)$ is a finite collection of functions, each of which is locally Lipschitz near x and also regular. Then, the function $f(x) := \max\{f_i(x) \mid i \in \{1, \ldots, N\}\}$ is regular at x, and

$$\partial f(x) = \mathrm{co}\{\partial f_i(x) \mid i \in I(x)\} \quad (73)$$

where $I(x)$ denotes the set of i for which $f_i(x) = f(x)$.

Proof: See [27, Prop. 2.3.12]. ∎

2) Lemmas to Prove Theorems 1 and 2

First, we show the lemmas which are used to prove both Theorems 1 and 2.

Lemma 1: Suppose that $-f$ is locally Lipschitz near x and regular for $f : \mathbb{R}^N \to \mathbb{R}$. Then, the right-directional derivative $f'(x; v)$ at x in the direction of $v \in \mathbb{R}^N$ satisfies

$$f'(x; v) = \min\{\zeta \cdot v \mid \zeta \in \partial f(x)\}. \quad (74)$$

Proof: For $\bar{f}(x) := -f(x)$, we have

$$f'(x; v) = -\bar{f}'(x; v) = -\bar{f}^o(x; v) \quad (75)$$

since $-f$ is regular. From Proposition 3, we have

$$\begin{aligned}\bar{f}^o(x; v) &= \max\{\zeta \cdot v \mid \zeta \in \partial \bar{f}(x)\} \\ &= \max\{\zeta \cdot v \mid \zeta \in -\partial f(x)\}\end{aligned} \quad (76)$$

since $\partial(-f(x)) = -\partial f(x)$ from Proposition 4. Thus

$$\begin{aligned}f'(x; v) &= -\bar{f}^o(x; v) = \min\{-\zeta \cdot v \mid \zeta \in -\partial f(x)\} \\ &= \min\{\zeta \cdot v \mid \zeta \in \partial f(x)\}.\end{aligned} \quad (77)$$

∎

Lemma 2: Let $S \subset \mathbb{R}^N$ be a nonempty closed convex set. Then, $\mathrm{Ln}(S)$ is a singleton and satisfies $\mathrm{Ln}(S)\cdot v \geq \|\mathrm{Ln}(S)\|^2$ for any $v \in S$.

Proof: In the case where $0 \in S$, it is clear that $\mathrm{Ln}(S)$ is a singleton, since $\mathrm{Ln}(S) = \{0\}$. For the proof in the case where $0 \notin S$, we assume that there exist $u_1, u_2 \in \mathrm{Ln}(S)$ where $u_1 \neq u_2$. Note that $u_1, u_2 \in \mathrm{Ln}(S)$ implies

$\|u_1\| = \|u_2\|$. Then, $u_1 \cdot u_2 < \|u_1\|\|u_2\|$, since $u_1 \neq u_2$ and $\|u_1\| = \|u_2\| \neq 0$ imply that the angle between u_1 and u_2 is not 0. Since S is a convex set, $u_3 := \frac{1}{2}(u_1 + u_2) \in S$. Thus, $\|u_3\|^2 = (\frac{1}{2}\|u_1 + u_2\|)^2 = \frac{1}{4}(\|u_1\|^2 + \|u_2\|^2 + 2u_1 \cdot u_2) < \frac{1}{4}(\|u_1\| + \|u_2\|)^2 = \|u_1\|^2$, which contradicts $u_1 \in \mathrm{Ln}(S)$. Therefore, $\mathrm{Ln}(S)$ is a singleton.

Next, we prove $\mathrm{Ln}(S) \cdot v \geq \|\mathrm{Ln}(S)\|^2$. In the case where $\mathrm{Ln}(S) = 0$, it clearly holds that $\mathrm{Ln}(S) \cdot v = 0, \forall v \in S$. In order to prove $u \cdot v \geq \|u\|^2, \forall v \in S$ for $u := \mathrm{Ln}(S) \neq 0$, we assume that there exists $v \in S$ which satisfies $u \cdot v < \|u\|^2$. Since S is convex, we have $w(a) := av + (1-a)u \subset S$ for any $a \in [0,1]$. However, since it holds that

$$\frac{d}{da}\|w(a)\| \bigg|_{a=0} = \frac{u \cdot v - \|u\|^2}{\|u\|} < 0 \tag{78}$$

we have $\|w(\varepsilon)\| < \|w(0)\| = \|u\|$ for a sufficiently small $\varepsilon > 0$, which contradicts $u = \mathrm{Ln}(S)$. Therefore, $u \cdot v \geq \|u\|^2$, which completes the proof. ■

Using Lemma 2, the following lemma is obtained for $\mathcal{U}_s$ in (33) and $\partial\mathcal{H}(V)$ in (30).

Lemma 3: For any $\zeta \in \partial\mathcal{H}(V)$, we have

$$\zeta \cdot \mathcal{U}_s \geq \frac{1}{\hat{K}} \min_{i \in I_H(V)} \|u_{si}\|^2. \tag{79}$$

Proof: From (30), any $\zeta \in \partial\mathcal{H}(V)$ can be written as

$$\zeta = \sum_{(i,j) \in I_F(V)} \lambda_{(i,j)} \nabla F_{(i,j)} + \sum_{(i,e) \in I_G(V)} \mu_{(i,e)} \nabla G_{(i,e)} \tag{80}$$

using $\{\lambda_{(i,j)}\}_{(i,j) \in I_F(V)}$ and $\{\mu_{(i,e)}\}_{(i,e) \in I_G(V)}$, which satisfy

$$\sum_{(i,j) \in I_F(V)} \lambda_{(i,j)} + \sum_{(i,e) \in I_G(V)} \mu_{(i,e)} = 1 \tag{81}$$

$$\lambda_{(i,j)} \geq 0, \forall (i,j) \in I_F(V), \mu_{(i,e)} \geq 0, \forall (i,e) \in I_G(V).$$

From $\mathcal{U}_s = [U_s^T, 0_{m+4}^T]^T$, we obtain

$$\nabla F_{(i,j)}(V) \cdot \mathcal{U}_s = \frac{\partial F_{(i,j)}}{\partial Q} U_s, \nabla G_{(i,e)}(V) \cdot \mathcal{U}_s = \frac{\partial G_{(i,e)}}{\partial Q} U_s.$$

Furthermore, the elements of $\frac{\partial F_{(i,j)}}{\partial Q}$ are 0, except for $\frac{\partial F_{(i,j)}}{\partial q_i}$ and $\frac{\partial F_{(i,j)}}{\partial q_j}$ in (66). Likewise, the elements of $\frac{\partial G_{(i,e)}}{\partial Q}$ are 0, except for $\frac{\partial G_{(i,j)}}{\partial q_i}$ in (67). Thus, we obtain

$$\zeta \cdot \mathcal{U}_s = \sum_{(i,j) \in I_F(V)} \frac{\lambda_{(i,j)}}{2} \left(\frac{q_i - q_j}{\|q_i - q_j\|} \cdot u_{si} + \frac{q_j - q_i}{\|q_j - q_i\|} \cdot u_{sj} \right) + \sum_{(i,e) \in I_G(V)} \mu_{(i,e)} \frac{q_i - \mathrm{Cp}_e(q_i)}{\|q_i - \mathrm{Cp}_e(q_i)\|} \cdot u_{si}. \tag{82}$$

For $i \in I_H(V)$, the input u_{si} in (14) can be written as

$$u_{si} = \hat{K} \cdot \mathrm{Ln}\left(\mathrm{co}\left(S_F \cup S_G\right)\right)$$
$$S_F = \left\{ \frac{q_i - q_j}{\|q_i - q_j\|} \,\middle|\, (i,j) \in I_F(V) \right\}$$
$$S_G = \left\{ \frac{q_i - \mathrm{Cp}_e(q_i)}{\|q_i - \mathrm{Cp}_e(q_i)\|} \,\middle|\, (i,e) \in I_G(V) \right\}. \tag{83}$$

From Lemma 2, it holds for any $(i,j) \in I_F(V)$ that

$$\frac{q_i - q_j}{\|q_i - q_j\|} \cdot u_{si} \geq \frac{\|u_{si}\|^2}{\hat{K}}, \frac{q_j - q_i}{\|q_j - q_i\|} \cdot u_{sj} \geq \frac{\|u_{sj}\|^2}{\hat{K}}$$

since $j \in I_H(V)$ if $(i,j) \in I_F(V)$. Thus, we have

$$\frac{1}{2}\left(\frac{q_i - q_j}{\|q_i - q_j\|} \cdot u_{si} + \frac{q_j - q_i}{\|q_j - q_i\|} \cdot u_{sj} \right) \geq \frac{1}{\hat{K}} \min_{i \in I_H(V)} \|u_{si}\|^2 \tag{84}$$

for any $(i,j) \in I_F(V)$. In the same way, it holds that

$$\frac{q_i - \mathrm{Cp}_e(q_i)}{\|q_i - \mathrm{Cp}_e(q_i)\|} \cdot u_{si} \geq \frac{\|u_{si}\|^2}{\hat{K}} \geq \frac{1}{\hat{K}} \min_{i \in I_H(V)} \|u_{si}\|^2 \tag{85}$$

for any $(i,e) \in I_G(V)$. By applying (81), (84), and (85) to (82), we obtain (79). ■

Next, we show the lemmas which are used to prove the first part of Theorem 1.

Lemma 4: For a finite number of continuous functions $f_k : \mathbb{R} \to \mathbb{R}$, $k \in \{1, \ldots, N\}$, we define $f(x) := \min_k f_k(x)$ and $I(x) := \{k \in \{1, \ldots, N\} \mid f_k(x) = f(x)\}$. Then, for each x, there exists $\delta > 0$, which satisfies

$$I(x') \subset I(x), \quad \forall x' \in B(x; \delta) \tag{86}$$

where $B(x;\delta) := \{x' : |x' - x| < \delta\}$.

Proof: In the case where $I^C(x) := \{k \in \{1, \ldots, N\} \mid f_k(x) \neq f(x)\} = \emptyset$ or $I(x) = \{1, \ldots, N\}$, it is clear that (86) is satisfied for any δ. Thus, we consider the case $I^C(x) \neq \emptyset$.

Suppose $I^C(x) = \{c_1, \ldots, c_k\}$ $(k < N)$. Then, $f_{c_j}(x) > f(x)$ for each j $(1 \leq j \leq k)$. Since $g_j(x') := f_{c_j}(x') - f(x')$ is a continuous function, there exists $\delta_j > 0$ which satisfies

$$| g_j(x') - d_j | < d_j, \quad \forall x' \in B(x; \delta_j) \tag{87}$$

where $d_j := g_j(x) = f_{c_j}(x) - f(x) > 0$. For such δ_j, it holds from (87) that $0 < g_j(x')$. Thus, we have $f_{c_j}(x') > f(x')$, which implies $c_j \in I^C(x')$. Therefore, for $\delta := \min_{j \in \{1,\ldots,k\}} \delta_j > 0$, we obtain

$$I^C(x) \subset I^C(x'), \quad \forall x' \in B(x; \delta) \tag{88}$$

which completes the proof due to $I^C(x) \subset I^C(x') \Leftrightarrow I(x') \subset I(x)$. ■

Lemma 5: There exits $T > 0$ which satisfies

$$I_F(V + \epsilon\mathcal{U}_s) \subset I_F(V)$$
$$I_G(V + \epsilon\mathcal{U}_s) \subset I_G(V), \forall \epsilon \in (0, T). \tag{89}$$

for any $q_i \in \mathrm{int}(\mathcal{P})$ and the corresponding u_{si} given in (14).

Proof: We number the elements of $\mathcal{IJ} \cup \mathcal{IE}$ such that

$$\phi_k \in \mathcal{IJ}, \quad \text{if } k = 1, \ldots, n(n-1)$$
$$\phi_k \in \mathcal{IE}, \quad \text{if } k = n(n-1)+1, \ldots, \bar{N} \tag{90}$$

where $\bar{N} := n(n+1) + nM$, and M is the number of edges of $\mathcal{P}$. Furthermore, we define the following sequence of a finite number of functions

$$f_k(\epsilon) := \begin{cases} F_{\phi_k}(V + \epsilon\mathcal{U}_s), & \text{if } k = 1, \ldots, n(n-1) \\ G_{\phi_k}(V + \epsilon\mathcal{U}_s), & \text{if } k = n(n-1)+1, \ldots, \bar{N}. \end{cases}$$

Then, from (9) and (26), we have

$$\mathcal{H}(V+\epsilon\mathcal{U}_s)=\min_k f_k(\epsilon). \tag{91}$$

Note that $F_{\phi_k}(V+\epsilon\mathcal{U}_s)$ and $G_{\phi_k}(V+\epsilon\mathcal{U}_s)$ are continuous functions of ϵ for fixed V and $\mathcal{U}_s$, since they each represent a distance between a fixed combination of two robots or a distance between a fixed combination of a robot and an edge. Thus, $f_k(\epsilon)$ is a continuous function of ϵ. It follows from Lemma 4 that there exists T such that

$$I(V+\epsilon\mathcal{U}_s)\subset I(V),\quad \forall\epsilon\in(0,T) \tag{92}$$

where $I(V+\epsilon\mathcal{U}_s):=\{k\in\{1,\dots,\bar{N}\}\mid f_k=\mathcal{H}(V+\epsilon\mathcal{U}_s)\}$. It is seen from the definitions of I_F and I_G in (31) that (92) is equivalent to

$$I_F(V+\epsilon\mathcal{U}_s)\cup I_G(V+\epsilon\mathcal{U}_s)\subset I_F(V)\cup I_G(V). \tag{93}$$

Therefore, the proof is completed, since $I_F(V+\epsilon\mathcal{U}_s)\cap I_G(V)=\emptyset$ and $I_G(V+\epsilon\mathcal{U}_s)\cap I_F(V)=\emptyset$. ■

Lemma 6: There exists T such that

$$\zeta\cdot\mathcal{U}_s\geq 0,\quad \forall\zeta\in\partial\mathcal{H}(V+\epsilon\mathcal{U}_s),\quad \forall\epsilon\in(0,T). \tag{94}$$

Proof: From (30), any $\zeta\in\partial\mathcal{H}(V+\epsilon\mathcal{U}_s)$ can be written as

$$\begin{aligned}\zeta\cdot\mathcal{U}_s=&\sum_{(i,j)\in I_F(V+\epsilon\mathcal{U}_s)}\lambda_{(i,j)}\nabla F_{(i,j)}(V+\epsilon\mathcal{U}_s)\cdot\mathcal{U}_s\\&+\sum_{(i,e)\in I_G(V+\epsilon\mathcal{U}_s)}\mu_{(i,e)}\nabla G_{(i,e)}(V+\epsilon\mathcal{U}_s)\cdot\mathcal{U}_s\end{aligned}$$

using $\{\lambda_{(i,j)}\}_{(i,j)\in I_F(V+\epsilon\mathcal{U}_s)}$ and $\{\mu_{(i,e)}\}_{(i,e)\in I_G(V+\epsilon\mathcal{U}_s)}$, which satisfy

$$\begin{aligned}&\sum_{(i,j)\in I_F(V+\epsilon\mathcal{U}_s)}\lambda_{(i,j)}+\sum_{(i,e)\in I_G(V+\epsilon\mathcal{U}_s)}\mu_{(i,e)}=1\\&\lambda_{(i,j)}\geq 0,\quad\forall(i,j)\in I_F(V+\epsilon\mathcal{U}_s)\\&\mu_{(i,e)}\geq 0,\quad\forall(i,e)\in I_G(V+\epsilon\mathcal{U}_s).\end{aligned}$$

From Lemma 5, $I_F(V+\epsilon\mathcal{U}_s)\subset I_F(V)$ for a sufficiently small $\epsilon>0$, which implies that any $(i,j)\in I_F(V+\epsilon\mathcal{U}_s)$ satisfies $(i,j)\in I_F(V)$. Thus, for any $(i,j)\in I_F(V+\epsilon\mathcal{U}_s)$, we have

$$(q_i-q_j)\cdot u_{si}+(q_j-q_i)\cdot u_{sj}\geq\frac{2}{\hat{K}}\|q_i-q_j\|\min_{i\in I_H(V)}\|u_{si}\|^2$$

in the same way as (84). Therefore

$$\begin{aligned}&\nabla F_{(i,j)}(V+\epsilon\mathcal{U}_s)\cdot\mathcal{U}_s\\&=\frac{1}{2}\frac{q_i+\epsilon u_{si}-q_j-\epsilon u_{sj}}{\|q_i+\epsilon u_{si}-q_j-\epsilon u_{sj}\|}\cdot(u_{si}-u_{sj})\\&=\frac{1}{2}\frac{(q_i-q_j)\cdot u_{si}+(q_j-q_i)\cdot u_{sj}+\epsilon\|u_{si}-u_{sj}\|^2}{\|q_i+\epsilon u_{si}-q_j-\epsilon u_{sj}\|}\geq 0\end{aligned}$$

for $(i,j)\in I_F(V+\epsilon\mathcal{U}_s)$.

Next, we need to show

$$\begin{aligned}\nabla G_{(i,e)}(V+\epsilon\mathcal{U}_s)\cdot\mathcal{U}_s&=\frac{q_i+\epsilon u_{si}-\mathrm{Cp}_e(q_i+\epsilon u_{si})}{\|q_i+\epsilon u_{si}-\mathrm{Cp}_e(q_i+\epsilon u_{si})\|}\cdot u_{si}\\&\geq 0\end{aligned} \tag{95}$$

for a sufficiently small ϵ. Since all the boundaries of D_L and D_R are included in D_M, it suffices to consider the cases of 1) $q_i\in D_L$ and $q_i+\epsilon u_{si}\in D_L$, 2) $q_i\in D_M$ and $q_i+\epsilon u_{si}\in D_M$, 3) $q_i\in D_R$, and $q_i+\epsilon u_{si}\in D_R$, for a sufficiently small ϵ.

In case 1, we have $\mathrm{Cp}_e(q_i+\epsilon u_{si})=\mathrm{Cp}_e(q_i)$ from the definition of Cp_e in (16). It follows that $(q_i+\epsilon u_{si}-\mathrm{Cp}_e(q_i+\epsilon u_{si}))\cdot u_{si}=(q_i-\mathrm{Cp}_e(q_i))\cdot u_{si}+\epsilon\|u_{si}\|^2$. Thus, it suffices to show $(q_i-\mathrm{Cp}_e(q_i))\cdot u_{si}\geq 0$ to show (95). From Lemma 5, $I_G(V+\epsilon\mathcal{U}_s)\subset I_G(V)$ for a sufficiently small $\epsilon>0$, which implies that any $(i,e)\in I_G(V+\epsilon\mathcal{U}_s)$ satisfies $(i,e)\in I_G(V)$. Thus, we have

$$(q_i-\mathrm{Cp}_e(q_i))\cdot u_{si}\geq\frac{1}{\hat{K}}\|q_i-\mathrm{Cp}_e(q_i)\|\min_{i\in I_H(V)}\|u_{si}\|^2\geq 0$$

in the same way as (85). Therefore, (95) has been proved in case 1). Note that the proof in case 3) is omitted since it is similar to case 1).

In case 2), it holds from the definition of Cp_e in (16) that

$$\mathrm{Cp}_e(q_i+\epsilon u_{si})=\mathrm{Cp}_e(q_i)+\frac{\epsilon u_{si}\cdot\bar{v}}{\|\bar{v}\|^2}\bar{v}$$

where $\bar{v}:=v_R-v_L$. Thus, we have

$$\begin{aligned}&(q_i+\epsilon u_{si}-\mathrm{Cp}_e(q_i+\epsilon u_{si}))\cdot u_{si}\\&=(q_i-\mathrm{Cp}_e(q_i))\cdot u_{si}+\epsilon\|u_{si}\|^2-\frac{\epsilon(u_{si}\cdot\bar{v})^2}{\|\bar{v}\|^2}\\&=(q_i-\mathrm{Cp}_e(q_i))\cdot u_{si}+\epsilon\frac{\|u_{si}\|^2\|\bar{v}\|^2-(u_{si}\cdot\bar{v})^2}{\|\bar{v}\|^2}.\end{aligned} \tag{96}$$

Since the last term in (96) is nonnegative, it suffices to show $(q_i-\mathrm{Cp}_e(q_i))\cdot u_{si}\geq 0$ to prove (95). From (14) and (83), S_i is a convex set and $\frac{q_i-\mathrm{Cp}_e(q_i)}{\|q_i-\mathrm{Cp}_e(q_i)\|}\in S_i$. It follows from Lemma 2 that $\mathrm{Ln}(S_i)\cdot\frac{q_i-\mathrm{Cp}_e(q_i)}{\|q_i-\mathrm{Cp}_e(q_i)\|}\geq\|\mathrm{Ln}(S_i)\|^2$. Thus, from (14), we have $u_{si}\cdot\frac{q_i-\mathrm{Cp}_e(q_i)}{\|q_i-\mathrm{Cp}_e(q_i)\|}\geq\|u_{si}\|^2/\hat{K}$, which implies $(q_i-\mathrm{Cp}_e(q_i))\cdot u_{si}\geq 0$. This concludes the proof of (95) in case of 2). ■

REFERENCES

[1] Y. U. Cao, A. S. Fukunaga, and A. B. Kahng, "Cooperative mobile robotics: Antecedents and directions," *Auton. Robots*, vol. 4, no. 1, pp. 7–23, 1997.

[2] T. Arai, E. Pagello, and L. E. Parker, "Editorial: Advances in multi-robot systems," *IEEE Trans. Robot. Autom.*, vol. 18, no. 5, pp. 655–661, Oct. 2002.

[3] R. M. Murray, "Recent research in cooperative control of multi-vehicle systems," *ASME J. Dyn. Syst., Meas., Control*, vol. 129, no. 5, pp. 571–583, 2007.

[4] M. A. Lewis and K.-H. Tan, "High precision formation control of mobile robots using virtual structures," *Auton. Robots*, vol. 4, no. 4, pp. 387–403, 1997.

[5] P. Ögren, M. Egerstedt, and X. Hu, "A control Lyapunov function approach to multiagent coordination," *IEEE Trans. Robot. Autom.*, vol. 18, no. 5, pp. 847–851, Oct. 2002.

[6] W. Ren and R. Beard, "Decentralized scheme for spacecraft formation flying via the virtual structure approach," *AIAA J. Guid., Control, Dyn.*, vol. 27, no. 1, pp. 73–82, 2004.

[7] P. K. C. Wang and F. Y. Hadaegh, "Coordination and control of multiple microspacecraft moving in formation," *J. Astronaut. Sci.*, vol. 44, no. 3, pp. 315–355, 1996.

[8] J. P. Desai, J. P. Ostrowski, and V. Kumar, "Modeling and control of formations of nonholonomic mobile robots," *IEEE Trans. Robot. Autom.*, vol. 17, no. 6, pp. 905–908, Dec. 2001.

[9] A. K. Das, R. Fierro, and V. Kumar, "A vision-based formation control framework," *IEEE Trans. Robot. Autom.*, vol. 18, no. 5, pp. 813–825, Oct. 2002.
[10] H. G. Tanner, G. J. Pappas, and V. Kumar, "Leader-to-formation stability," *IEEE Trans. Robot. Autom.*, vol. 20, no. 3, pp. 443–455, Jun. 2004.
[11] H. Fukushima, K. Kon, and F. Matsuno, "Model predictive formation control using branch-and-bound compatible with collision avoidance problems," *IEEE Trans. Robot.*, vol. 29, no. 5, pp. 1308–1317, Oct. 2013.
[12] D. V. Dimarogonas, M. Egerstedt, and K. J. Kyriakopoulos, "A leader-based containment control strategy for multiple unicycles," in *Proc. IEEE Conf. Decis. Control*, 2006, pp. 5968–5973.
[13] M. Ji, G. Ferrari-Trecate, M. Egerstedt, and A. Buffa, "Containment control in mobile networks," *IEEE Trans. Autom. Control*, vol. 53, no. 8, pp. 1972–1975, Sep. 2008.
[14] T. Balch and R. C. Arkin, "Behavior-based formation control for multirobot teams," *IEEE Trans. Robot. Autom.*, vol. 14, no. 6, pp. 926–939, Dec. 1998.
[15] L. E. Parker, "ALLIANCE: An architecture for fault tolerant multirobot cooperation," *IEEE Trans. Robot. Autom.*, vol. 14, no. 2, pp. 220–240, Apr. 1998.
[16] M. Schneider-Fontán and M. J. Matarić, "Territorial multi-robot task division," *IEEE Trans. Robot. Autom.*, vol. 14, no. 5, pp. 815–822, Oct. 1998.
[17] R. Olfati-Saber, "Flocking for multi-agent dynamic systems: Algorithms and theory," *IEEE Trans. Autom. Control*, vol. 51, no. 3, pp. 401–420, Mar. 2006.
[18] H. Su, X. Wang, and Z. Lin, "Flocking of multi-agents with a virtual leader," *IEEE Trans. Autom. Control*, vol. 54, no. 2, pp. 293–307, Feb. 2009.
[19] C. Belta and V. Kumar, "Abstraction and control for groups of robots," *IEEE Trans. Robot.*, vol. 20, no. 5, pp. 865–875, Oct. 2004.
[20] N. Michael and V. Kumar, "Planning and control of ensembles of robots with nonholonomic constraints," *Int. J. Robot. Res.*, vol. 28, no. 8, pp. 962–975, Aug. 2009.
[21] C. C. Cheah, S. P. Hou, and J. J. E. Slotine, "Region-based shape control for a swarm of robots," *Automatica*, vol. 45, no. 10, pp. 2406–2411, 2009.
[22] S. P. Hou and C. C. Cheah, "Dynamic compound shape control of robot swarm," *IET Control Theory Appl.*, vol. 6, no. 3, pp. 454–460, 2012.
[23] T. Kamegawa, T. Yamasaki, H. Igarashi, and F. Matsuno, "Development of the Snake-like Rescue Robot "KOHGA, "" in *Proc. IEEE Int. Conf. Robot. Autom.*, New Orleans, LA, USA, Apr. 2004, pp. 5081–5086.
[24] H. Fukushima, S. Satomura, T. Kawai, M. Tanaka, T. Kamegawa, and F. Matsuno, "Modeling and control of a snake-like robot using the screw-drive mechanism," *IEEE Trans. Robot.*, vol. 28, no. 3, pp. 541–554, Jun. 2012.
[25] R. Ariizumi, H. Fukushima, and F. Matsuno, "Front-unit-following control of a snake-like robot using screw drive mechanism based on past velocity commands," in *Proc. IEEE/RSJ Int. Conf. Intell. Robot. Syst.*, Sep. 2011, pp. 1907–1912.
[26] J. Cortés and F. Bullo, "Coordination and geometric optimization via distributed dynamical systems," *SIAM J. Control Optim.*, vol. 44, no. 5, pp. 1543–1574, 2005.
[27] F. H. Clarke, *Optimization and Nonsmooth Analysis*. New York, NY, USA: Wiley, 1983.
[28] D. Shevitz and B. Paden, "Lyapunov stability theory of nonsmooth systems," *IEEE Trans. Autom. Control*, vol. 39, no. 9, pp. 1910–1914, Sep. 1994.
[29] A. Bacciotti and F. Ceragioli, "Stability and stabilization of discontinuous systems and nonsmooth Lyapunov functions," *ESAIM: Control, Optim. Calculus Variat.*, vol. 4, pp. 361–376, 1999.
[30] A. F. Filippov, *Differential Equations With Discontinuous Righthand Sides*. Dordrecht, The Netherlands: Kluwer, 1988.

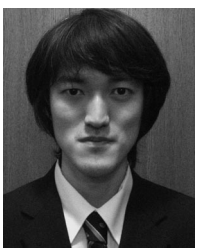

Kazuya Yoshida received the B.S. and M.S. degrees in engineering from the University of Electro-Communications, Tokyo, Japan, in 2009 and 2011, respectively. His Master's degree focused on formation control of multirobot systems.

He is currently with Caterpillar Japan ltd., Tokyo.

Hiroaki Fukushima (M'06) received the B.S. and M.S. degrees in engineering, and the Ph.D. degree in informatics, from Kyoto University, Kyoto, Japan, in 1995, 1998, and 2001, respectively.

From 1999 to 2004, he was a Research Fellow of Japan Society for the Promotion of Science. From 2001 to 2003, he was a Visiting Scholar with the University of California at San Diego, LaJolla, CA, USA. From 2004 to 2009, he was a Research Associate and an Assistant Professor with the University of Electro-Communications, Japan. He is currently an Assistant Professor with Kyoto University. His research interests include system identification and robust control.

Dr. Fukushima received the ISCIE Young Author Award in 2001 and the SICE paper award in 2003. He is a member of the Society of Instrument and Control Engineers; the Institute of Systems, Control, and Information Engineers; and the Robotics Society of Japan.

Kazuyuki Kon (S'07–M'10) received the B.S. and M.S. degrees in engineering from the University of Electro-Communications, Tokyo, Japan, in 2005 and 2007, respectively, and the Ph.D. degree in engineering from Kyoto University, Kyoto, Japan, in 2010.

From 2009 to 2011, he was a Research Fellow with Japan Society for the Promotion of Science. He is currently an Assistant Professor with Kyoto University. His research interests include autonomous mobile robots and formation control.

Fumitoshi Matsuno (M'94) received the Ph.D. (Dr. Eng.) degree from Osaka University, Osaka, Japan, in 1986.

In 1986, he joined the Department of Control Engineering, Osaka University. He became a Lecturer in 1991 and an Associate Professor in 1992 with the Department of Systems Engineering, Kobe University, Kobe, Japan. In 1996, he joined the Department of Computational Intelligence and Systems Science, Interdisciplinary Graduate School of Science and Engineering, Tokyo Institute of Technology, Tokyo, Japan, as an Associate Professor. In 2003, he became a Professor with the Department of Mechanical Engineering and Intelligent Systems, University of Electro-Communications. Since 2009, he has been a Professor with the Department of Mechanical Engineering and Science, Kyoto University, Kyoto, Japan. He holds also the post of Vice President with NPO International Rescue System Institute. His current research interests include robotics, swarm intelligence, control of distributed parameter and nonlinear systems, and rescue support systems during disasters.

Dr. Matsuno has received many awards, including the Outstanding Paper Award in 2001 and 2006, Takeda Memorial Prize in 2001 from the Society of Instrument and Control Engineers (SICE), and the Best Paper Award in 2013 from Information Processing Society of Japan. He is a Fellow member of the SICE and the Japan Society of Mechanical Engineers and a member of the RSJ and the Institute of Systems, Control, and Information Engineers, among other organizations. He served as a Cochair of IEEE Robotics and Automation Society Technical Committee on Safety, Security, and Rescue Robotics, a chair of the Steering Committee of the SICE Annual Conference, a General Chair of IEEE SSRR2011 and IEEE/SICE SII2011, etc. He is an Editor-in-Chief of the *Journal of RSJ*, an Editor of the *Journal of Intelligent and Robotic Systems*, an Associate Editor of *Advanced Robotics*, the *International Journal of Control, Automation, and Systems*, etc., and on the Conference Editorial Board of the IEEE Control Systems Society.